MISSOURI S&T | CURTIS LAWS WILSON LIBRARY
MISSOURI UNIVERSITY OF SCIENCE AND TECHNOLOGY

Scholars' Mine

Doctoral Dissertations | Student Theses and Dissertations

Summer 2009

Spacecraft formation flight at sun-earth/moon libration points

Douglas Robert Tolbert

Follow this and additional works at: https://scholarsmine.mst.edu/doctoral_dissertations

 Part of the Aerospace Engineering Commons

Department: Mechanical and Aerospace Engineering

Recommended Citation

Tolbert, Douglas Robert, "Spacecraft formation flight at sun-earth/moon libration points" (2009). *Doctoral Dissertations*. 2266.
https://scholarsmine.mst.edu/doctoral_dissertations/2266

This thesis is brought to you by Scholars' Mine, a service of the Missouri S&T Library and Learning Resources. This work is protected by U. S. Copyright Law. Unauthorized use including reproduction for redistribution requires the permission of the copyright holder. For more information, please contact scholarsmine@mst.edu.

SPACECRAFT FORMATION FLIGHT

AT SUN-EARTH/MOON

LIBRATION POINTS

by

DOUGLAS ROBERT TOLBERT

A DISSERTATION

Presented to the Faculty of the Graduate School of the

MISSOURI UNIVERSITY OF SCIENCE AND TECHNOLOGY

In Partial Fulfillment of the Requirements for the Degree

DOCTORATE OF PHILOSOPHY IN AEROSPACE ENGINEERING

2009

Approved by

Henry J. Pernicka, Advisor
David W. Riggins
S.N. Balakrishnan
Joshua Rovey
Gerald Wilemski

COPYRIGHT 2009

Douglas Robert Tolbert
All Rights Reserved

ABSTRACT

Formations of spacecraft, positioned near the libration points of the Sun-Earth/Moon system, have recently received an increase in interest in response to a variety of mission needs. Specifically, missions such as the Micro Arcsecond X-Ray Imaging Mission (MAXIM), Terrestrial Pathfinder (TPF), Stellar Imager (SI) and the European Space Agency's DARWIN all baseline formations of spacecraft to satisfy mission requirements. Replacing the traditional single spacecraft mission with multiple small spacecraft flying in formation is advantageous for these missions, especially when establishing a virtual aperture. These types of formations allow for higher resolution observations than with a single, conventional aperture. The de-emphasis on a single monolithic spacecraft approach to spacecraft mission design also reduces the chance of catastrophic failure of the mission if a single spacecraft can no longer perform its duty.

The present study focuses on the relative dynamics of spacecraft within a formation orbiting near a libration point, such as L_2 as examined in this study. A method for finding, understanding, and then exploiting the natural dynamics near a libration point for formation flight is sought. Various formation types (relative halo orbit, fixed-position, and paraboloid) are examined to determine the feasibility of natural formations for various applications.

A method for determining possible $\Delta\mathbf{V}$ magnitudes and time between $\Delta\mathbf{V}$ maneuvers is also sought to gain an understanding of possible controlled formations that simultaneously exploit the natural dynamics while also controlling the spacecraft in the formation. One approach was identified that uses impulsive maneuvering at specified times to control the spacecraft in the formation desired.

ACKNOWLEDGMENTS

I would like to thank the Missouri University of Science and Technology for providing me with a quality engineering education, providing me with the opportunity to grow as a student and a person and providing financial assistance during my entire graduate career. I would especially like to thank Dr. Pernicka for being a fantastic advisor and a great teacher. I would also like to express my thanks to committee for aiding me in my graduate career and serving on my committee. I'd like to thank my lovely wife for her constant support and help. I wouldn't have been able to do it without her. Finally, I would like to thank my family for their constant support throughout my entire academic career.

TABLE OF CONTENTS

Page

LIST OF ILLUSTRATIONS

LIST OF TABLES

NOMENCLATURE

Symbol	Description
m_i	Mass of Body (Earth/Moon, Sun, spacecraft)
M^*	Sum of Mass of Bodies
R	Distance from Earth/Moon to Sun
L^*	Distance from Earth/Moon to Sun for Nondimensionalization
μ	Gravitational Parameter for Earth/Moon System
a	Semimajor Axis
G	Gravitational Constant for System
G^*	Gravitational Constant for System Nondimensionalization
t	Time
T^*	Time for Nondimensionalization
n	Mean Motion of System
n^*	Mean Motion of System for Nondimensionalization
ϑ	Angle of System
$\dot{\vartheta}$	Angular Rate of System
$\ddot{\vartheta}$	Angular Acceleration of System
T	Kinetic Energy
V	Potential Energy
x	Position along the x-axis of the System
y	Position along the y-axis of the System
z	Position along the z-axis of the System
$\dot{x}$	Velocity along the x-axis of the System
$\dot{y}$	Velocity along the y-axis of the System
$\dot{z}$	Velocity along the z-axis of the System
$\ddot{x}$	Acceleration along the x-axis of the System
$\ddot{y}$	Acceleration along the y-axis of the System
$\ddot{z}$	Acceleration along the x-axis of the System

r_i	Radial Distance Between Two Bodies
L	Lagrangian
u	Pseudo Potential
A	Matrix of Partial Derivatives
ϕ	State Transition Matrix

1. INTRODUCTION

1.1. OVERVIEW

Replacing the traditional single spacecraft mission with multiple small spacecraft flying in formation can be advantageous for many missions. This de-emphasis on a single monolithic spacecraft approach to spacecraft mission design reduces the chance of catastrophic failure of the mission if a single spacecraft can no longer perform its duty. This approach also "promotes agility, adaptability, evolvability, scalability, and affordability through the exploitation of multiple space platforms."[1]

A primary motivation in the development of formation flying techniques is the maintenance of a virtual aperture used for observing distant objects in space. "A virtual aperture is an effective aperture generated by a cluster of physically independent elements."[1] These types of formations allow for higher resolution observations than with a single, conventional aperture.

1.2. DISTRIBUTED SPACE SYSTEMS

Distributed Space Systems (DSS) is a concept involving multi-spacecraft formations. As more advanced spacecraft operational capabilities are required to accomplish innovative scientific missions, a shift to the incorporation of Distributed Space Systems needs to be developed. DSS also represents an important shift in overall mission design. One area of focus is the relative dynamics of spacecraft within a formation orbiting about a libration point.

Formation flying has been defined as the tracking or maintenance of a desired relative separation, orientation, or position between or among spacecraft.[6] DSS is a more specific type of formation where the relative separations, orientations or positions are of particular interest and importance to the mission for scientific purposes. For most missions, a single, monolithic spacecraft contains all of the important spacecraft hardware and operations are duplicated onboard to prevent catastrophic mission failure. Alternatively, some new missions emphasize the requirement of multiple spacecraft maintaining a specific and known set of relative parameters.

One of these mission concepts is interferometry[3]. Interferometry uses a virtual aperture created from multiple spacecraft flying in a formation to observe the same object (of scientific interest) in space. Maintaining a specific formation of spacecraft for a virtual aperture used for observing objects in space is a primary motivation in the development of formation flying techniques. A virtual aperture is an effective aperture generated by a cluster of physically independent elements working together, which is where DSS comes into consideration.

1.3. PREVIOUS WORK

In reviewing the state-of-the-art in spacecraft formation flight at libration points, previous contributions are first summarized below from the general categories of "Basic Libration Point Dynamics" and "Trajectory Control at Libration Points." The review is then narrowed to consideration of past efforts with spacecraft formation flight (including primarily Earth orbiters). The literature survey concludes with a discussion of those works involving libration point formation flight specifically.

1.3.1. Basic Libration Point Dynamics. The classic text by Szebeheley[4] established the foundation for the restricted three-body problem and facilitated much of the progress with libration point orbit research in the 1960s and 1970s. Following the publication of his text, considerable work was accomplished in finding both analytical and numerical solutions for orbits about libration points. Farquhar[5] derived analytical solutions for quasi-periodic orbits for the translunar libration point using the Lindstedt-Poincaré method. Included within his solutions are the effects of nonlinearities, lunar orbital eccentricity, and the solar gravitation field. He identified methods of determining the minimum amplitude required of the in-plane motion to guarantee a corresponding out-of-plane amplitude that will produce a path where the frequencies of each motion are equal, thus producing a halo orbit (as opposed to a Lissajous orbit).

Richardson[6-8] sought a fourth-order analytical solution for periodic motion about the collinear points of the Circular Restricted Three-Body Problem (CR3BP). He was able to obtain all four orders of the nonlinear solution using recursive relationships. The solution was constructed by using a method of successive approximations coupled with a technique similar to the Lindstedt-Poincaré method. This was useful for the ISEE-3

mission[9], the first such mission to use a halo orbit, where the analytical solution was used as the initial approximation followed by the use of numerical methods.

Continued development of the families of orbits around the collinear points was performed by Howell[10]. She expanded the effort to better understand these orbits by numerically determining halo families of orbits. She found that the halo families of periodic orbits extend from the libration points to the nearest primary and that they appeared to exist for all values of the mass ratio of the two primaries. It was also shown that the L_2 and L_3 families of orbits have very similar characteristics to each other.

In the previous studies by Richardson[6], Lissajous trajectories associated with the collinear libration points in the restricted three-body problem were successfully computed analytically to at least fourth-order. Those approximations were utilized by Howell and Pernicka[11] to determine such trajectories numerically for an arbitrary, predetermined number of revolutions in the rotating frame. Such trajectories were constructed in various primary systems, for a wide range of orbit sizes and a large number of revolutions.

1.3.2. Trajectory Control at Libration Points. Cielaszyk and Wie[12] treated the inherent nonlinearities present as trajectory-dependent, persistent disturbance inputs to be incorporated in a linear state-feedback controller for the computation of trajectories near libration points. This method was then used as a fuel-efficient nominal path. They then went on to show that the method could also be used iteratively to generate large, complex, quasi-periodic Lissajous trajectories.

Gurfil and Meltzer[13] developed new methods for generating periodic orbits at collinear libration points and for stabilizing the motion. They introduced a continuous acceleration control term into the state-space dynamics to find linear periodic reference trajectories. In this system, linearization about the libration points in pulsating coordinates yields an unstable linear parameter-varying system. The nonlinear terms of the equations of motion were treated as periodic disturbances and a disturbance accommodating control was used to track the reference trajectory in the presence of nonlinear periodic disturbances.

Rahmani[14] et al. approached the problem by using optimal control theory, implementing a variation of the extremals technique to solve the two point boundary

value problem. Their approach utilized fully nonlinear equations of motion in order to more closely approximate real world scenarios.

A number of efforts address the problem of stationkeeping libration point trajectories. A comprehensive survey paper by Dunham and Roberts[15] provides a good summary of techniques.

1.3.3. Spacecraft Formation Flight. Much of the past research accomplished in the area of spacecraft formation flight has been applied to geocentric mission design. The current body of literature contains many citations regarding Earth-orbiting formation flight[16-19]. Some of these concepts extend to libration point formations, but due to the unique dynamics of the three-body problem, much of the geocentric state-of-the-art is not directly applicable at libration points. Nonetheless, it remains of value to study these concepts for what they can offer to the proposed research in hopes of gaining an understanding on the natural dynamics.

1.3.4. Libration Point Formation Flight. Recent years have seen an increase in Sun-Earth L_2 libration point mission studies due to the considerable interest in formation flight in this region. Orbits about the L_2 point are valued for their observational potential of distant objects from this region. With a spacecraft moving about the L_2 point the Sun, Earth, and Moon all appear in the same general direction, facilitating enhanced strategies for reducing the interference radiating from these bodies during data collection. This location also places the formation out of Earth's geomagnetic tail.

Formation flying has been defined as "the tracking or maintenance of a desired relative separation, orientation, or position between or among spacecraft."[20] Replacing traditional single large spacecraft with formations of multiple small spacecraft can be advantageous in many mission architectures. This decentralized approach in spacecraft mission design reduces the chance of catastrophic failure in one spacecraft significantly impairing the function of the formation as a whole. This approach also "promotes agility, adaptability, evolvability, scalability, and affordability through the exploitation of multiple space platforms."[21] A primary motivation in the development of formation flying techniques is the maintenance of a virtual aperture used for observing distant objects in space. "A virtual aperture is an effective aperture generated by a cluster of

physically independent elements."[21] These types of formations allow for higher resolution observations than with a single conventional aperture.

There are several technological challenges involved in implementing these types of formation missions. One is providing accurate and affordable relative tracking of individual spacecraft in the formation. Another is that in the mission design of virtual aperture formations, observational modes of operations have been defined that require the relative positions of each spacecraft in the formation to be controlled as tightly as one centimeter within their nominal separations[22, 23]. Such a requirement creates the challenge of identifying hardware that can produce thrust controllable to very low magnitudes with sufficient accuracy to maintain the formation within this error tolerance.

Research in this area has focused on the development of control strategies involving both continuous and discrete thrusting techniques[24-28]. Previous examinations of discrete techniques[29, 30] examined the problem by dividing the trajectory into segments of a given time with impulsive maneuvers performed to maintain that path within a certain allowable error bound. Marchand and Howell[29, 30] found that ΔV magnitudes in this region for small formation displacements and allowed error bounds can be prohibitively small for the given state-of-the-art in propulsion technologies.

The focus of the study[31] by Carlson, Pernicka, and Balakrishnan was on the use of impulsive maneuvers to maintain formation flight at a libration point, and in particular, formation sizes and control tolerances were sought for which impulsive maneuvering becomes a practical option. However, in recent years, increasing interest in DSS and the required low thrust levels have promoted advances in the development of propulsive devices that can produce very low thrust. One example of this promising technology is the development of colloid micro-Newton cold gas thrusters with thrust levels in the 5-30 μN range[32]. For smaller spacecraft (~100 kg) planned for DSS missions such as the Stellar Imager, this results in an approximate attainable ΔV range of $1x10^{-6}$ to $1x10^{-5}$ m/s with an approximate resolution of $1x10^{-4}$ m/s. While all the necessary lifetime and performance testing have not been completed it appears that ΔV values in this range will be feasible in the near future. Additionally, a very recent announcement[33] has been made by the European Space Agency (ESA) concerning a new Field Emission Electric Propulsion (FEEP) engine that can generate thrust in the range of 0.1 - 150

micronewtons, with a resolution capability better than 0.1 micronewtons and a time response of one-fifth of a second (190 milliseconds) or better. Given a spacecraft mass of around one hundred kilograms, that translates to a $\Delta\mathbf{V}$ on the order of $1x10^{-9}$ – $1x10^{-8}$ m/s. with an error tolerance near $1x10^{-9}$ m/s.

In the area of continuous thrust, a new control technique was investigated[34, 35] for the circular restricted three-body problem with the Sun and Earth as the two primaries. The leader spacecraft is maintained in the nominal orbit around the L_2 libration point. A virtual structure concept is used as a framework for multiple spacecraft formation in which the center of the virtual rigid body is assumed to follow a nominal orbit around the L_2 libration point. Control is applied to each individual spacecraft to maintain a constant relative distance from the center of the virtual structure. A nonlinear model was developed that describes the relative formation dynamics. This nonlinear control problem was addressed by using a new nonlinear control approach, called the *ϑ-D* technique. This method is based upon the optimal control concept and provides a closed-form suboptimal feedback solution. In this approach, a solution to the Hamiltonian-Jacobi-Bellman (HJB) equation is approximated by including a finite number of perturbations in the series solution.

Infeld[36] et al. use a concurrent approach to formation control in which the formation design and control aspects are combined. While their results appear promising, it is unclear whether onboard computers would possess the necessary computational resources to implement their algorithms to effectively control the formation at the centimeter level.

Collange and Leitner[37] focused on the natural motion of two spacecraft at the L_2 libration point with the assumption of a circular restricted three-body problem where disturbances and nongravitational effects were ignored. They examined the natural motion's influence on fuel consumption over long periods as opposed to controlled motion, which has previously received considerable attention. Their focus was on determining formations that are primarily governed by natural gravitational effects such that maintenance of the formation over the long-term will not require significant fuel consumption.

With the considerable focus on the collinear libration points dynamics, navigation and control, little attention has been given to the triangular libration points. Recently, Catlin and McLaughlin[38, 39] explore the dynamics of relative motion near the Earth-Moon L_4 point within the circular restricted three body problem, where they concluded that formations are possible at the Earth-Moon triangular points on uncontrolled trajectories.

1.4. CURRENT STUDY

The present study focuses on the relative dynamics of spacecraft within a formation orbiting near a libration point. For the scope of the present research, L_2 was the libration point of choice. A method is sought for finding, understanding, and then exploiting the natural dynamics near a libration point for formation flight. Motivation for this research stems from a NASA Goddard Spaceflight Center research announcement[44] where research was sought in the area of feasibility for aspherical formations near the Sun-Earth/Moon L_2 libration point. The primary specification used from this announcement was the one centimeter error bound on the formation relative positions. Additional specifications were outlined in the research announcement such as length of formation pointing, formation rotation and a maneuver mode but are not in the present scope of this research. Various formation types (relative halo orbit, fixed-position, and paraboloid) are examined to determine the feasibility of natural formations for various applications with emphasis on interferometry

Additionally, a method for determining $\Delta\mathbf{V}$ magnitudes and the time between $\Delta\mathbf{V}$ maneuvers is also explored in order to gain an understanding of possible controlled formations that simultaneously exploit the natural dynamics while also controlling the spacecraft in the formation. This method uses impulsive maneuvering at specified times to control the spacecraft in the formation desired.

1.5. ORGANIZATION

Following this introductory section, the remainder of the document is organized as follows:

- Section 2 – This section provides a background of the three-body problem and the dynamic model used.

- Section 3 – This section gives a detailed description of the assumptions and methods built into the study along with a detailed analysis of the results obtained for the various formation sizes and geometries explored.

- Section 4 – This section gives conclusions based on the results and discusses future research.

2. BACKGROUND

2.1. RESTRICTED THREE-BODY PROBLEM

An important first step for the present investigation was the selection of the model used to represent the dynamics of the spacecraft motion. For this study, the assumptions of the Circular Restricted Three-Body Problem (CR3BP) were chosen.

2.1.1. Libration Points in the Three-Body Problem. In the 3BP, a single spacecraft's motion is assumed to only be influenced by two primary bodies. For this study, the larger primary was the Sun (m_1) and the smaller primary was the Earth/Moon (m_2) system. The Earth/Moon system is treated as a single body whose mass is equal to the sum of the Earth and Moon and is located at the barycenter of the Earth/Moon system. Figure 2.1 illustrates the various Lagrange points (also known as libration points) for the Sun-Earth/Moon system (note this figure is not to scale).

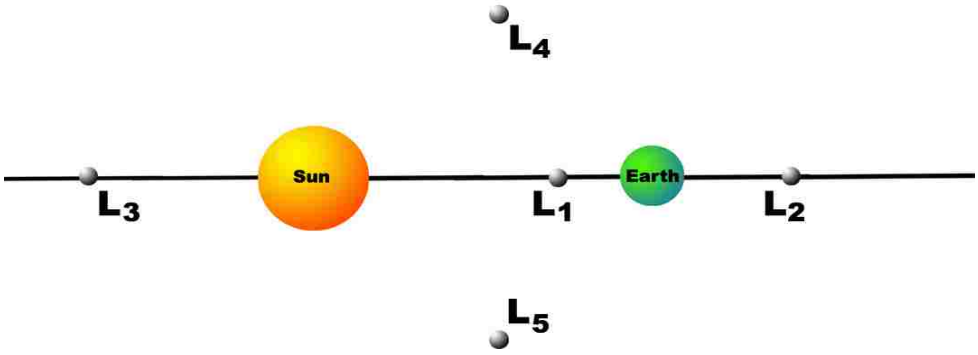

Figure 2.1. Libration Point Illustration

Libration points are equilibrium points in space. They occur where the velocity and acceleration components of a third body, relative to the rotating frame, are zero. There are three collinear libration points (L_1, L_2, and L_3) and two triangular libration points (L_4 and L_5). The collinear libration points lie along a line drawn through the Sun and Earth/Moon mass center. The triangular libration points form equilateral triangles with the Sun and Earth/Moon in the plane of motion of the primaries. One difference between the collinear and triangular points is that the collinear points are unstable, while the triangular points are stable for certain mass ratios of the primaries m_1 and m_2.

Each individual libration point has potential for various types of missions. The L_1 and L_3 points are well-suited for solar observation missions. The natural stability of the L_4 and L_5 triangular points is an aspect which may some day be exploited in a scientific mission.

2.1.2. Circular Restricted Three-Body Problem Assumptions. The Circular Restricted Three-Body Problem (CR3BP) assumes that the two primaries rotate about their barycenter in a circle. Several assumptions were built into the CR3BP model for ease in generating equations of motion for the third mass (m_3). In the derivation of the equations of motion (EOMs), nondimensionalization is performed. An additional benefit of nondimensionalizing is a simplified set of EOMs

The first two steps set the sum of the two primary masses, m_1 and m_2, and the distance between the two primaries, R, equal to one nondimensional unit as shown in equations (1) and (2).

$$\frac{m_1 + m_2}{M^*} = 1 \tag{1}$$

$$\frac{R}{L^*} = 1 \tag{2}$$

The distance between the two primaries, R, is also equal to the semimajor axis of the primary system as shown in equation (3).

$$R = a = 149{,}597{,}870.66 \text{ km} = 1 \text{ AU} \tag{3}$$

Using equations (2) and (3) a conversion can be developed to apply to the initial conditions to convert distance measurements from kilometers to nondimensional units and to convert velocities from kilometers per second to nondimensional units.

$$L^* = 149{,}597{,}870.66 \text{ km} \tag{4}$$

$$M^* = 1.989006\text{x}10^{30} \text{ kg} \tag{5}$$

The third step in the process is to define a unit of time, *T**, so that *G** (the nondimensional universal gravitational constant) is equal to one. Using T* as the time unit in *G* results in a value of *G** equal to one nondimensional unit. Furthermore, as shown in equation (7) factoring equation (6) produces an expression for *T** equal to the inverse of the mean motion of the Sun-Earth/Moon system which is a known quantity. The mean motion is defined as the angular frequency of the system.

$$G^* = 1 = G\frac{(m_1 + m_2)(T^*)^2}{a^3} \tag{6}$$

$$T^* = \left[\frac{a^3}{G(m_1 + m_2)}\right]^{1/2} = 1/n \tag{7}$$

where $n = 1.9906405695\text{x}10^{-7}$ rad/s and $G = 6.67x10^{-20}\frac{\text{km}^3}{\text{kg}\cdot\text{s}^2}$

This results in a value of *T** as

$$\text{T}^* = 1/n = 5{,}023{,}508.5896 \text{ seconds} = 58.1424605 \text{ days} \tag{8}$$

The nondimensional mean motion of the primary system is shown to also be equal to one through

$$n^* = \left[\frac{G^* M^*}{(L^*)^3}\right]^{1/2} = 1 \tag{9}$$

In the CR3BP problem the angular rate and angular acceleration of the rotating frame are then

$$\dot{\theta} = n^* = 1 \tag{10}$$

$$\ddot{\theta} = 0 \tag{11}$$

2.1.3. Dynamical Model. Figure 2.1 shows the geometry of the Restricted Three-Body Problem. In many studies, the rotating reference frame is defined with origin at the libration point of interest or at the barycenter of the two-body system. In either case, the $\hat{\mathbf{x}}$ unit vector is typically directed from the larger primary toward the smaller primary. The $\hat{\mathbf{y}}$ unit vector is defined normal to the $\hat{\mathbf{x}}$ vector, within the plane of the primaries' orbit, and along the prograde rotational direction. The $\hat{\boldsymbol{z}}$ unit vector then completes the right-handed frame and is thus normal to the plane of the primaries' orbit. Based on this coordinate system, the kinetic energy, *T*, and potential energy, *V*, can be defined for an arbitrary spacecraft orbiting a libration point as

$$T = \frac{1}{2} m_3 \left[\left(\dot{x} - \dot{\theta} y \right)^2 + \left(\dot{y} + \dot{\theta} x \right)^2 + \dot{z}^2 \right] \tag{12}$$

$$V = \frac{-G\left(m_3 m_1\right)}{r_1} - \frac{G m_3 m_2}{r_2} \tag{13}$$

The variables $\boldsymbol{r_1}$ and $\boldsymbol{r_2}$ are defined in equation (14).

$$\begin{aligned} \boldsymbol{r_1} &= \left(x + \mu R \right) \hat{\boldsymbol{x}} + y \hat{\boldsymbol{y}} + z \hat{\boldsymbol{z}} \\ \boldsymbol{r}_2 &= \left[x - \left(1 - \mu \right) R \right] \hat{\boldsymbol{x}} + y \hat{\boldsymbol{y}} + z \hat{\boldsymbol{z}} \end{aligned} \tag{14}$$

Now, define the Langragian for the system as

$$L = T - V \tag{15}$$

Based on equation (15), the EOMs for the (conservative) system can then be derived using Lagrange's equation

$$\frac{d}{dt}\left(\frac{\partial L}{\partial \dot{q}_j}\right) - \frac{\partial L}{\partial q_j} = 0 \tag{16}$$

If the spacecraft is located by a position vector **r** with base point at the barycenter using coordinates *x*, *y*, and *z* with respect to the rotating frame, then the nondimensional equations of motion (assuming the primaries orbit *elliptically*) are given as

$$\begin{aligned}
\ddot{x} - 2\dot{\theta}\dot{y} - \ddot{\theta}y - \dot{\theta}^2 x &= \frac{-(1-\mu)(x+\mu R)}{r_1^{\,3}} - \frac{\mu(x-(1-\mu)R)}{r_2^{\,3}} \\
\ddot{y} + 2\dot{\theta}\dot{x} + \ddot{\theta}x - \dot{\theta}^2 y &= \frac{-(1-\mu)y}{r_1^{\,3}} - \frac{\mu y}{r_2^{\,3}} \\
\ddot{z} &= \frac{-(1-\mu)z}{r_1^{\,3}} - \frac{\mu z}{r_2^{\,3}}
\end{aligned} \tag{17}$$

where $\dot{\theta}$ is the angular rate of the rotating frame (constant in the CR3BP), μ is the ratio of the smaller primary mass to the sum of the masses of both primaries, R is the distance (equal to one nondimensional unit in the CR3BP) between the primaries, and r_1 and r_2 are the distances from the larger and smaller primary to the spacecraft, respectively. The term $\ddot{\theta}$ is the magnitude of the angular acceleration of the rotating frame and in the case of the CR3BP is zero. Figure 2.2 illustrates the coordinate frames and relative distances for the three bodies.

Figure 2.2. Basic Geometry of the Restricted Three-Body Problem

The EOMs can be simplified for the CR3BP due to the mean motion becoming a constant value (unity) and take the form

$$\begin{aligned} \ddot{x} - 2\dot{y} - x &= \frac{-(1-\mu)(x+\mu R)}{r_1^3} - \frac{\mu(x-(1-\mu)R)}{r_2^3} \\ \ddot{y} + 2\dot{x} - y &= \frac{-(1-\mu)y}{r_1^3} - \frac{\mu y}{r_2^3} \\ \ddot{z} &= \frac{-(1-\mu)z}{r_1^3} - \frac{\mu z}{r_2^3} \end{aligned} \tag{19}$$

With the equations of motion defined above, the next step was to find solutions. The three second order differential equations were expressed as six first order differential equations in the form

$$f_1 = \dot{x}$$

$$
\begin{aligned}
f_2 &= \dot{y} \\
f_3 &= \dot{z} \\
f_4 &= \ddot{x} = \frac{\partial u}{\partial x} + 2\dot{y} \\
f_5 &= \ddot{y} = \frac{\partial u}{\partial y} - 2\dot{x} \\
f_6 &= \ddot{z} = \frac{\partial u}{\partial z}
\end{aligned}
\tag{20}
$$

where u is defined as the pseudo potential

$$
u = \frac{1}{2}\dot{\theta}^2(x^2 + y^2) + \frac{1-\mu}{r_1} + \frac{\mu}{r_2} \tag{21}
$$

Next, the matrix of partial derivatives was defined as

$$
A = \begin{bmatrix}
\frac{\partial f_1}{\partial x} & \frac{\partial f_1}{\partial y} & \frac{\partial f_1}{\partial z} & \frac{\partial f_1}{\partial \dot{x}} & \frac{\partial f_1}{\partial \dot{y}} & \frac{\partial f_1}{\partial \dot{z}} \\
\frac{\partial f_2}{\partial x} & & & & & \cdots \\
\frac{\partial f_3}{\partial x} & & & & & \\
\frac{\partial f_4}{\partial x} & & & & & \\
\frac{\partial f_5}{\partial x} & & & & & \\
\frac{\partial f_6}{\partial x} & \cdots & & & & \frac{\partial f_6}{\partial \dot{z}}
\end{bmatrix}
=
\begin{bmatrix}
0 & 0 & 0 & 1 & 0 & 0 \\
0 & 0 & 0 & 0 & 1 & 0 \\
0 & 0 & 0 & 0 & 0 & 1 \\
\frac{\partial^2 u}{\partial x^2} & \frac{\partial^2 u}{\partial x \partial y} & \frac{\partial^2 u}{\partial x \partial z} & 0 & 2 & 0 \\
\frac{\partial^2 u}{\partial x \partial y} & \frac{\partial^2 u}{\partial y^2} & \frac{\partial^2 u}{\partial y \partial z} & -2 & 0 & 0 \\
\frac{\partial^2 u}{\partial x \partial z} & \frac{\partial^2 u}{\partial y \partial z} & \frac{\partial^2 u}{\partial z^2} & 0 & 0 & 0
\end{bmatrix}
\tag{22}
$$

With the matrix of partial derivatives defined, an approximate (linear) relationship between changes in the initial states (position and velocity) of the spacecraft to the final states at a specified end time is now available. This relationship between states at different times gives rise to a differential corrections method that allows for the possibility of modifying initial states to achieve specific end states. The differential

corrections method described next, is then used to generate initial conditions that generate nominal libration point orbits based on desired end state parameters.

2.1.4. Simulation. MATLAB was used to simulate the trajectories in this study. The MATLAB function "ode113" was used to numerically integrate the equations of motion for every spacecraft. The ode113 function is a variable order Adams-Bashforth-Moulton PECE multistep solver - it needs the solutions at several (usually two) preceding time points to compute the current solution. The minimum error tolerances used with the numerical integration were an absolute error tolerance of $1\text{x}10^{-13}$ and a relative error tolerance of $1\text{x}10^{-13}$ which corresponds to precision on the distance of approximately 14.95 micrometers and a velocity precision of approximately 2.98 nanometers per second.

2.2. THE DIFFERENTIAL CORRECTIONS METHOD

One important tool used in this research was the differential corrections method. The differential corrections method makes use of the state transition matrix, ϕ, which linearly relates changes in initial states to changes in final states at a specified end time through the relationship

$$\begin{Bmatrix} x_o \\ y_o \\ z_o \\ \dot{x}_o \\ \dot{y}_o \\ \dot{z}_o \end{Bmatrix}_{Desired} - \begin{Bmatrix} x_o \\ y_o \\ z_o \\ \dot{x}_o \\ \dot{y}_o \\ \dot{z}_o \end{Bmatrix}_{Actual} = \phi^{-1}\left(t_f, t_o\right) \cdot \left[\begin{Bmatrix} x_f \\ y_f \\ z_f \\ \dot{x}_f \\ \dot{y}_f \\ \dot{z}_f \end{Bmatrix}_{Desired} - \begin{Bmatrix} x_f \\ y_f \\ z_f \\ \dot{x}_f \\ \dot{y}_f \\ \dot{z}_f \end{Bmatrix}_{Actual} \right] \tag{23}$$

The state transition matrix is computed by numerically integrating the linear state transition matrix differential equation

$$\frac{d\phi\left(t_f, t_o\right)}{dt} = A(t)\phi\left(t_f, t_o\right) \tag{24}$$

where

$$\varphi(t_f, t_0) = I \tag{25}$$

with I being the identity matrix.

After propagating the spacecraft orbit from a given initial state to a final state, equation (23) can be used to generate corrections to the initial spacecraft states to cause a desired resulting change in the final states. Equation (24) is used to propagate the state-transition-matrix $\phi(t_f, t_o)$ simultaneously with the equations of motion (1) with $\phi(0,0)$ set equal to the identity matrix. This process can also proceed in the opposite direction, allowing the calculation of resulting changes in the initial states for desired changes in the final states. Since this is a linear approximation applied to the nonlinear motion, the differential corrections must be applied iteratively to converge to a solution. Various differential corrections techniques were implemented in this research and are explained in more detail in subsequent sections.

3. NATURAL ORBITS AND FORMATIONS

3.1. PERIODIC ORBITS

It would be useful to find naturally periodic orbits near Earth for desirable communication, gravitational and thermal considerations. In this light, orbits near the Sun-Earth/Moon L_2 are sought. An infinite number of periodic solutions exist in the Circular Restricted Three-Body Problem (CR3BP). Quasi-periodic orbits known as Lissajous[4] trajectories exist near libration points. Halo[6, 7] orbits are a special class of Lissajous orbits and form a particular set of periodic solutions to the CR3BP that are also symmetric about the x-z-plane. The CR3BP EOMs cannot be solved explicitly in general closed-form so halo orbits are of particular interest in their ability to aid in the understanding of the solutions of the EOMs.

3.1.1. Lissajous Orbits. Lissajous orbits are quasi-periodic solutions to the equations of motion of the CR3BP. Previous research has developed methods for computing these orbits using both analytical approximations and numerical methods. References 5 and 6 demonstrate an analytical approach for computing Lissajous orbits. Howell and Pernicka[11] developed a numerical method to determine nominal Lissajous orbits. The focus for the research presented in this paper was on halo orbits, a subset of Lissajous orbits.

3.1.2. Halo Orbits. Halo orbits are a special class of Lissajous orbits that are naturally periodic around the collinear libration points (L_2 used in this study). References 7 and 8 provide analytical approximation approaches and reference 10 provides a numerical approach for computing halo orbits. The motion of a spacecraft in a halo orbit about a libration point is inherently unstable and eventually it will drift away from its nominal orbit about the libration point.

Due to the unstable nature of halo and Lissajous orbits, the trajectories require station-keeping. Control maneuvers must be used to maintain a spacecraft on a specific orbit for long periods of time. Due to these station-keeping control maneuvers, natural orbits that minimize fuel consumption and/or maximize time spent without performing a control maneuver are of particular interest.

In computing the leader spacecraft's nominal halo orbit, a differential corrections technique was implemented. The spacecraft starts with the y-position equal to zero and then x-velocity and z-velocity equal to zero so that the spacecraft will begin moving perpendicular to the x-z plane. The spacecraft initial z-position and y-velocity were differentially corrected to satisfy specified conditions at time equal to exactly half the halo orbit period. Due to the symmetry in the CR3BP EOMs, it could then be assumed the spacecraft would follow the mirror image of that trajectory on its second half. The requirements for the final states were an x-velocity and z-velocity equal to zero when the spacecraft next crossed the y-axis. In other words, the spacecraft needed to cross perfectly perpendicular to the x-z plane. Because it is impossible to cross the x-z plane perfectly perpendicular due to numerical limitations and because of the instability inherent to orbits near libration points, the spacecraft will need to be controlled (stationkept) throughout the orbit.

In order to generate the leader spacecraft's reference halo orbit in the CR3BP, an analytical approximation was implemented to generate a "good" initial guess for use with the fully nonlinear EOMs in computing numerical solutions. For the current study, the following initial conditions relative to L_2 were used to generate a numerically integrated halo orbit about the libration point.

$$\begin{Bmatrix} x_o \\ y_o \\ z_o \end{Bmatrix} = \begin{Bmatrix} 87{,}028.50933 \\ 0 \\ -191{,}234.00018 \end{Bmatrix} \text{ km}$$

$$\begin{Bmatrix} \dot{x}_o \\ \dot{y}_o \\ \dot{z}_o \end{Bmatrix} = \begin{Bmatrix} -8.93698856 \\ -109.55806459 \\ 10.02007061 \end{Bmatrix} \frac{\text{km}}{\text{s}}$$

Initially, the position and velocity were specified and the differential corrections method was used to modify the initial conditions (z-position and y-velocity) to generate a halo orbit. The final result (based on the "good" initial guess) was the initial conditions listed above. Figure 3.1 illustrates the three-dimensional orbit in three two-dimensional projections. The star at the center denotes the L_2 libration point location. Appendix A

contains additional figures that aid in visualizing the halo orbit and give detailed information on the spacecraft's states as functions of time. This nominal halo orbit is treated as the leader spacecraft's reference orbit. All follower spacecraft orbits are then defined with respect to the leader's reference orbit. It is noted that the leader spacecraft's trajectory is now considered a known quantity at all times. Additionally, any position relative to the leader spacecraft is also considered known. This is useful when follower spacecraft are placed into orbits with respect to the leader spacecraft and a nominal trajectory for the follower spacecraft must be available.

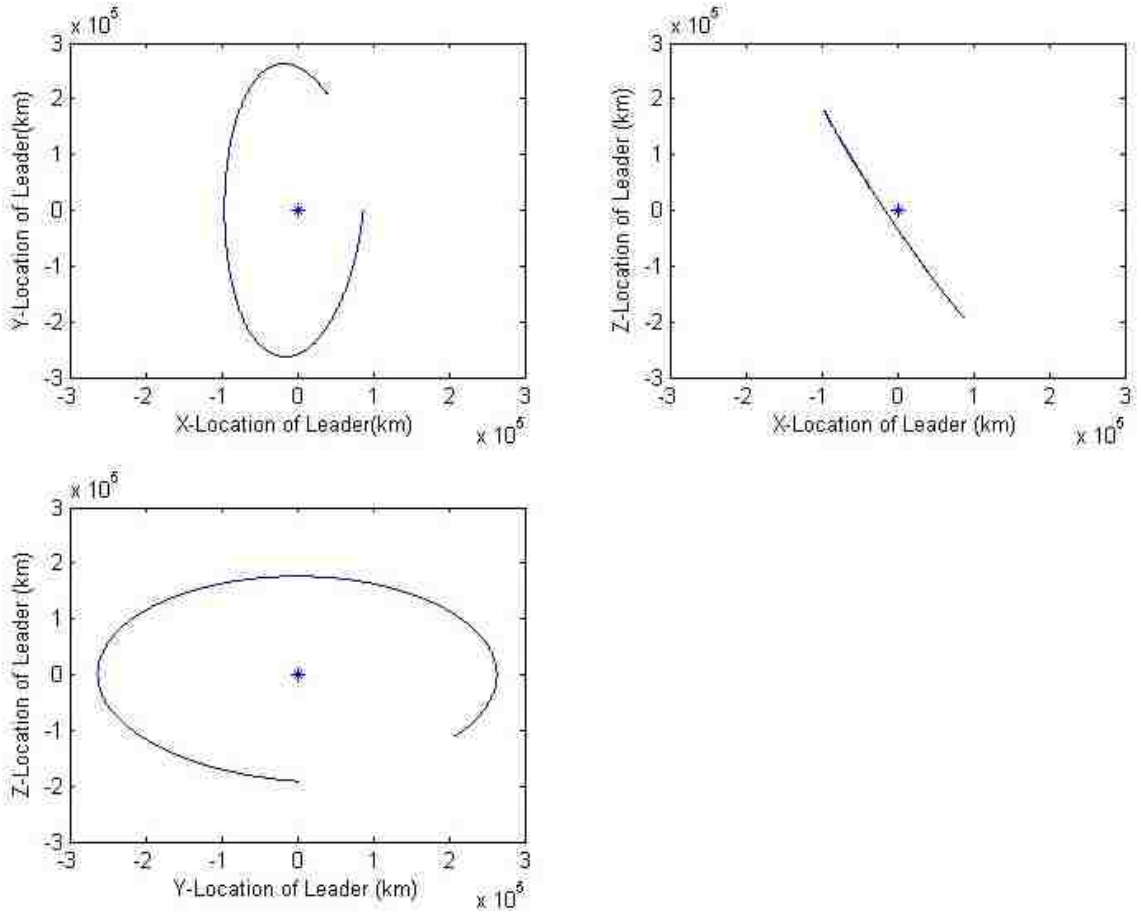

Figure 3.1. Two-Dimensional Projections of Leader Spacecraft Halo Orbit

3.2. FORMATION FLIGHT

With the leader spacecraft initial states and nominal trajectory defined, the next step was to introduce a single follower spacecraft. The follower spacecraft also orbits the

libration point and has a specified initial position relative to the leader spacecraft. Various types of formations could be used to address specific mission needs, typically determined by scientific requirements (as opposed to commercial and military, which to date have not yet identified libration formation flight as an area of interest). An example of current missions that are utilizing or will utilize formations of spacecraft are the Micro Arc-second X-ray Imaging Mission (MAXIM) [41], Terrestrial Planet Finder (TPF), Stellar Imager (SI) and the European Space Agency's DARWIN[42]. These missions call for different formation requirements and formation types and were used as baselines for the current study. In order to gain a greater understanding of the natural dynamics near the Sun-Earth/Moon L_2 libration point in light of the above missions, three different formation types were examined: relative halo orbits, fixed position and paraboloid surface. Each formation type has unique properties and scientific uses. For purposes of this study, the individual spacecraft's attitude dynamics and control were not addressed.

3.2.1. Relative Halo Orbits. The first formation considered was a follower spacecraft that orbited the leader spacecraft in its own relative halo orbit. Segerman[40] has shown that the linearized equations of motion of one spacecraft relative to another take the same form as that of a single spacecraft moving about a collinear libration point. In other words, the follower spacecraft moves in a halo orbit about the leader spacecraft while the leader spacecraft orbits the libration point in its nominal halo orbit.

Due to the relatively long period of a halo orbit (on the order of 180 days for the leader and follower spacecraft), the leader and follower spacecraft both appear to be following very similar halo orbits about the libration point in the rotating frame but the follower spacecraft will actually be orbiting the leader spacecraft in its own relative halo orbit. Initially, the follower spacecraft is placed in various relative positions with respect to the leader with an initial relative velocity of zero in order to find a relative position that will naturally generate a halo orbit relative to the leader spacecraft. This is accomplished by propagating the follower spacecraft initial conditions and examining its trajectory to determine its suitability as a follower spacecraft traveling on a halo orbit relative to the leader spacecraft.

The first step in determining an initial position of the follower spacecraft that lends itself to a natural relative halo orbit was to place spacecraft in various positions

relative to the leader and examine their behavior over at least half the period of the leader spacecraft's halo orbit. Next, the follower spacecraft's trajectories were examined over their entire trajectories to determine which initial positions maintained a close proximity to the leader spacecraft.

Through trial-and-error, it was determined that a minimum of fourteen different locations relative to the leader spacecraft were required to adequately ascertain neighborhoods of relative positions that yielded acceptable natural dynamics (by maintaining close proximity to the leader). These fourteen starting positions were all at a fixed distance magnitude relative to the leader spacecraft but placed at varying locations surrounding the leader spacecraft. For the initial case, the distance magnitude was arbitrarily set at ten kilometers.

The fourteen points were generated by specifying the eight points of intersection between a sphere surrounding the leader spacecraft and a cube with the leader spacecraft at the center and the six points that are defined by normals to each face of the cube that intersect the sphere. The cube was arranged, for convenience, in such a way that one of the three initial positions coordinates was equal to zero. In other words, eight of the cases examined were when the initial x-position and the initial y-position were each set equal to zero. This was convenient for the case of relative halo orbits such that some of the initial positions had a relative y-component equal to zero for purposes of finding relative halo orbits. These eight points defined the cube's corners. The other six cases were then based on the normals of the six sides of the cube. Table 3.1 contains the initial coordinates for the fourteen cases.

It should be noted that this process was performed to gain a quick, qualitative understanding of the nature of the dynamics between the leader spacecraft and the possible positions of the follower spacecraft and was not an exhaustive quantitative analysis of all relative starting positions for the follower spacecraft possible. A more detailed examination of relative starting positions for a follower spacecraft would need to be made based on particular mission requirements.

Table 3.1. Initial Coordinates of Follower Spacecraft

	X (km)	Y (km)	Z (km)
1	7.07107	0	7.07107
2	7.07107	0	-7.07107
3	**-7.07107**	**0**	**7.07107**
4	-7.07107	0	-7.07107
5	0	7.07107	7.07107
6	0	7.07107	-7.07107
7	0	-7.07107	7.07107
8	0	-7.07107	-7.07107
9	7.07107	7.07107	0
10	7.07107	-7.07107	0
11	-7.07107	7.07107	0
12	-7.07107	-7.07107	0
13	0	0	10
14	0	0	-10

Of the fourteen cases, the case with an initial positive x-position, zero y-position and a negative z-position (highlighted) gave the "best" natural halo orbit. Appendix B contains various figures that illustrate the process of choosing the best neighborhood for starting positions of follower spacecraft to yield halo orbits. In order to help visualize this process, only the eight points that made up the corners of the cube were plotted on the figures. Each of the fourteen cases was examined to find the one that most closely followed a similar orbit to the leader spacecraft.

Similar to the process of finding initial conditions for the leader spacecraft, the follower spacecraft is given an initial position as defined above and the same differential corrections technique used in Section 3.1.2 to generate the leader spacecraft's halo orbit is used to correct the follower's initial conditions to generate a halo orbit relative to the leader. It should be noted that the differential corrections technique used alters the initial z-position and the initial y-velocity. Due to this change in the initial z-position (because of the differential corrections technique implemented), the spacecraft is not at the same initial position. The follower spacecraft moved 1.25 kilometers along the z-axis, changing to distance magnitude by 0.84 kilometers, deemed acceptable in this study. The initial conditions for the follower spacecraft are defined below.

$$\begin{Bmatrix} x_o \\ y_o \\ z_o \end{Bmatrix} = \begin{Bmatrix} 7.07107 \\ 0 \\ -5.82811 \end{Bmatrix} \text{ km}$$

$$\begin{Bmatrix} \dot{x}_o \\ \dot{y}_o \\ \dot{z}_o \end{Bmatrix} = \begin{Bmatrix} 0 \\ 0.0105919 \\ 0 \end{Bmatrix} \frac{\text{km}}{\text{s}}$$

Once the spacecraft has had its initial conditions corrected such that a halo orbit is generated, a new differential corrections technique (described below) was implemented. It was necessary to generate a new differential corrections technique because the follower spacecraft needed to remain at a fixed position relative to the leader spacecraft, as only its initial velocity should be changed in order to preserve the formation geometry. Thus, the new technique allows the follower spacecraft to be differentially corrected to find a proper halo orbit without affecting its initial position. The new technique takes advantage of the information gained through the original differential corrections process (the position where the spacecraft crosses the y-axis) to generate a slightly different halo orbit with a specified initial position.

The new differential corrections technique differs from the previous one used by altering the three initial velocities and targeting an exact position. The primary motivation behind developing a new differential corrections technique was a desire to not change the initial position of the follower spacecraft once it had been chosen so a follower spacecraft could be placed at any specified initial position. Instead, the initial position remained fixed and only the initial velocities were differentially corrected in order to target a specific end state position. The desired end state position was not known until the original differential corrections technique was used. For this case, the end state condition specified was the final state position of the spacecraft at half the halo orbit period after using the original differential corrections method. In other words, the spacecraft trajectory was originally corrected by altering the z-position and y-velocity and targeting an x-velocity and z-velocity of zero when the spacecraft passes through the x-z plane. It should be noted that in changing the initial velocities of the follower

spacecraft, the follower will no longer be on a truly periodic halo orbit. By definition, when the spacecraft crosses the x-z plane, it should have an x-velocity and z-velocity equal to zero. By making their initial x-velocity and z-velocity nonzero, the follower is no longer on a halo orbit. Differential corrections (with corresponding deterministic ΔVs) will need to be applied at every half period.

Based on this original differential corrections method, a specific reference halo orbit was found. The end state position values (taken at the half period) were taken from this reference solution and used as the target states for a new follower spacecraft that starts at an initial position required by the mission, not necessarily the same initial position as the reference follower. With the initial position defined, the new differential corrections technique was free to find different initial velocities that would yield the same end state position from the reference solution. For this case, the differential corrections technique converged on the solution in three iterations with a tolerance on the nondimensional end state positions of $1\text{x}10^{-13}$ (on the order of two centimeters). The "new" initial states for the follower spacecraft were determined to be

$$\begin{Bmatrix} x_o \\ y_o \\ z_o \end{Bmatrix} = \begin{Bmatrix} 7.07107 \\ 0 \\ -7.07107 \end{Bmatrix} \text{ km}$$

$$\begin{Bmatrix} \dot{x}_o \\ \dot{y}_o \\ \dot{z}_o \end{Bmatrix} = \begin{Bmatrix} -0.00003412 \\ 0.0110258 \\ 0.00000281 \end{Bmatrix} \frac{\text{km}}{\text{s}}$$

The follower spacecraft now starts out at a specified initial position and targets a generated end state position by changing its initial velocities. The resultant relative halo orbit can be seen in Figure 3.2. The three illustrations portray the motion of the follower in two dimensions with the star denoting the leader position. It should be noted that instabilities that make the leader spacecraft halo orbit sensitive also affect the follower spacecraft. As can be seen in Figure 3.2, the follower starts to drift away from the nominal orbit before it completes a full revolution. The approximate period for the follower spacecraft's relative halo orbit is 179 days (time of the half period was 89.46

days). Since it does not complete a full revolution, its orbital period is not exact. The maximum distance the follower spacecraft was from the leader spacecraft was on the order of forty kilometers (note the follower spacecraft started at ten kilometers away from the leader spacecraft).

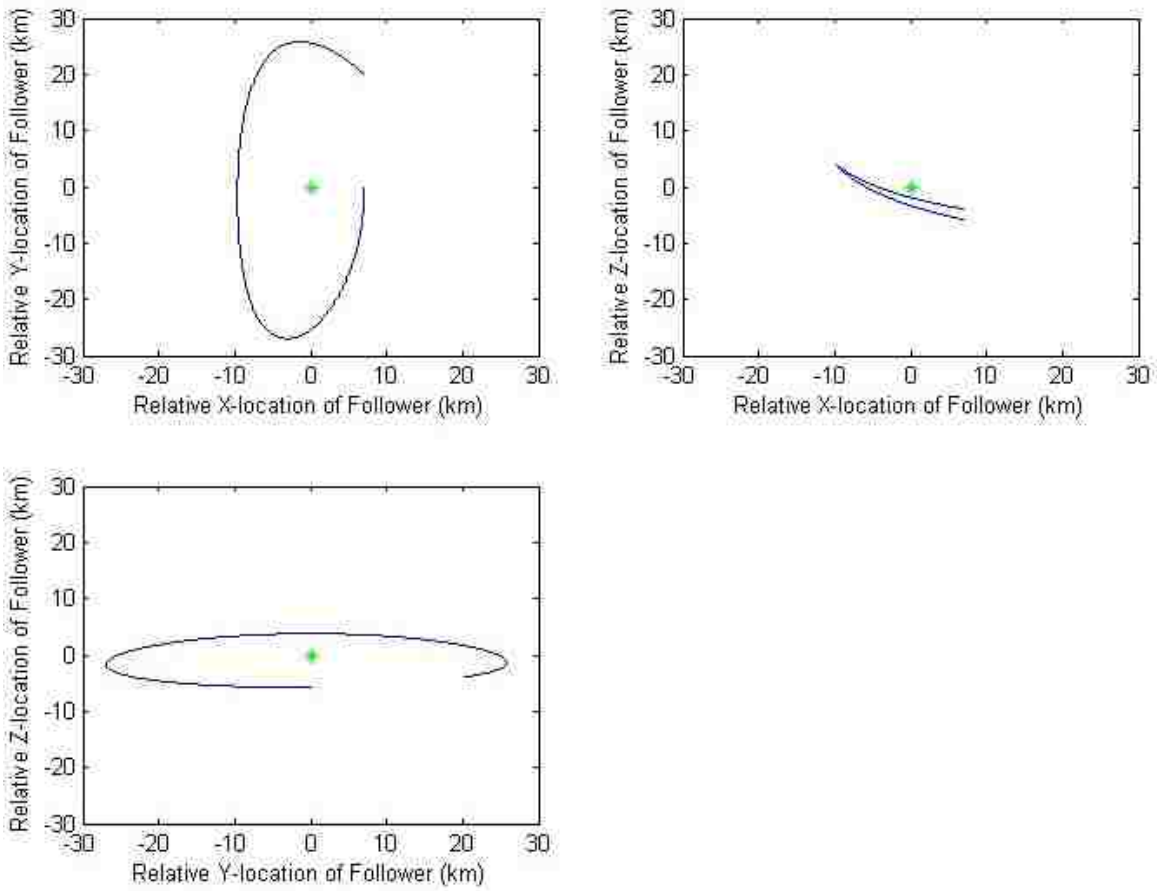

Figure 3.2. Relative Halo Orbit of Follower Spacecraft

3.2.2. Relative Halo Orbit Formations. With a follower halo orbit defined, the next step was to incorporate additional follower spacecraft. As a first attempt at establishing a formation, the additional follower spacecraft were simply added at $t = 0$ in the simulation along the trajectory (given the same states) of the original reference follower at roughly equal spacing along the orbit. However, in the fully three-dimensional sense, the additional follower spacecraft now start in a different point in space compared to where they "should" be. In other words, while the additional follower

spacecraft may be in correct relative positions along the reference halo orbit, they actually start out in different points in the inertial frame compared to where that relative position was along the reference trajectory. For example, the location along the follower's reference trajectory that corresponds to thirty days into the orbit is in a different inertial location due to the fact that the leader spacecraft has also moved during the thirty days. This difference causes the divergence of the additional follower spacecraft trajectories as seen in Figure 3.3. Each star represents an initial position for the four different cases considered (0, 30, 50 and 100 days).

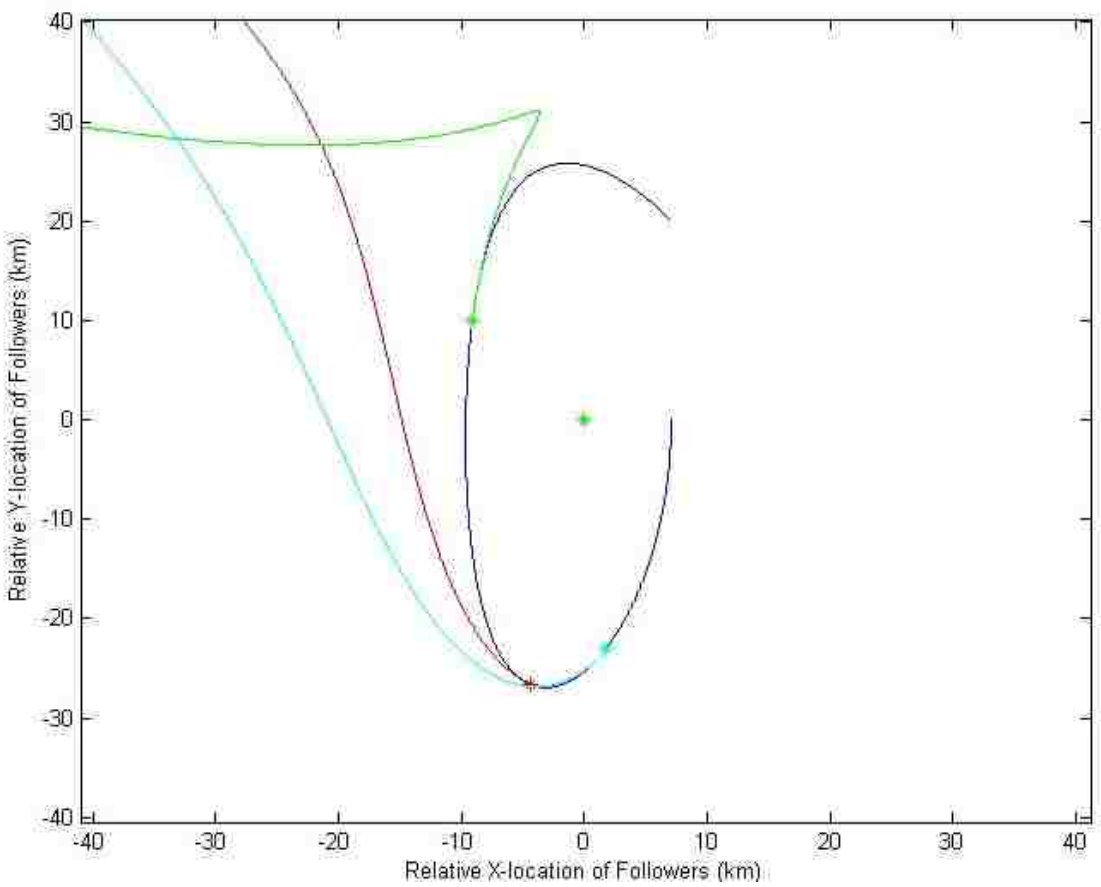

Figure 3.3. Relative Orbits of Additional Follower Spacecraft

With the initial starting positions for the four additional follower spacecraft defined, the next step was to differentially correct the additional follower spacecraft' initial conditions. The original goal was for the additional follower spacecraft to follow the same trajectory as the reference follower. The first thought was to change the

additional follower spacecraft's initial velocities until the trajectories followed the same relative halo orbit path. In fact, the natural dynamics created a situation where it was impossible to generate initial velocities while maintaining the same initial positions that would yield the same trajectory as the follower reference orbit. This situation arose because as the leader spacecraft traveled along its halo orbit, the positions relative to it were also changing in the inertial frame. Thus, the follower spacecraft's relative halo orbits were directly influenced by time due to their dependence on the position of the leader spacecraft (which is moving along its own halo orbit). This effect was large enough to influence the follower spacecrafts' relative orbits significantly and cause them to drift from the reference trajectory.

As stated above, the first attempt was to differentially correct the additional followers' initial velocities and target the three dimensional position in space. An additional constraint of forcing the time of flight from the initial position to the final position to be the same as the reference orbit was implemented. Unfortunately, due to the nature of the dynamics around a libration point, the additional followers did not follow the reference trajectory. A specific example of this can be seen in Figure 3.4 with initial position at the reference orbit's thirty day location. As demonstrated by Figure 3.4, it was possible to get *similar* orbits that followed trajectories that were close to the reference orbit but it was not possible to generate specific initial conditions that would lead to the *same* trajectory for any starting position. With this understanding, additional differential corrections techniques were sought.

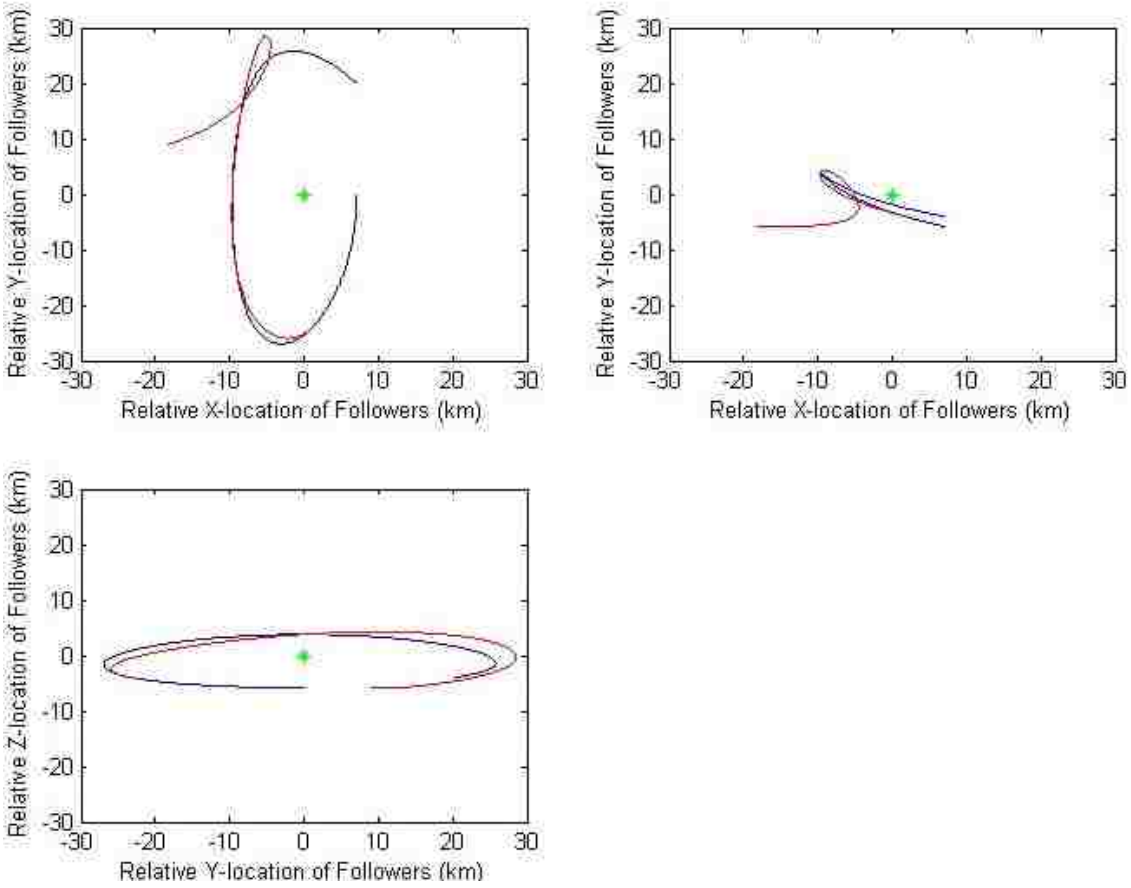

Figure 3.4. Differentially Corrected Relative Halo Orbit

Because the method of targeting a specific location did not produce desired results, an alternative differential corrections method was developed. This third method targeted a specific y-position, x-velocity and z-velocity. The goal was to have the spacecraft pass through the same x-position (z-position was free to change) as the reference follower while also crossing that x-position with no relative x-velocity and z-velocity. Figure 3.5 illustrates this attempt. As can be seen below, this third (and final) differential corrections method did not successfully find any initial conditions that would yield a relative halo orbit that matched the reference orbit.

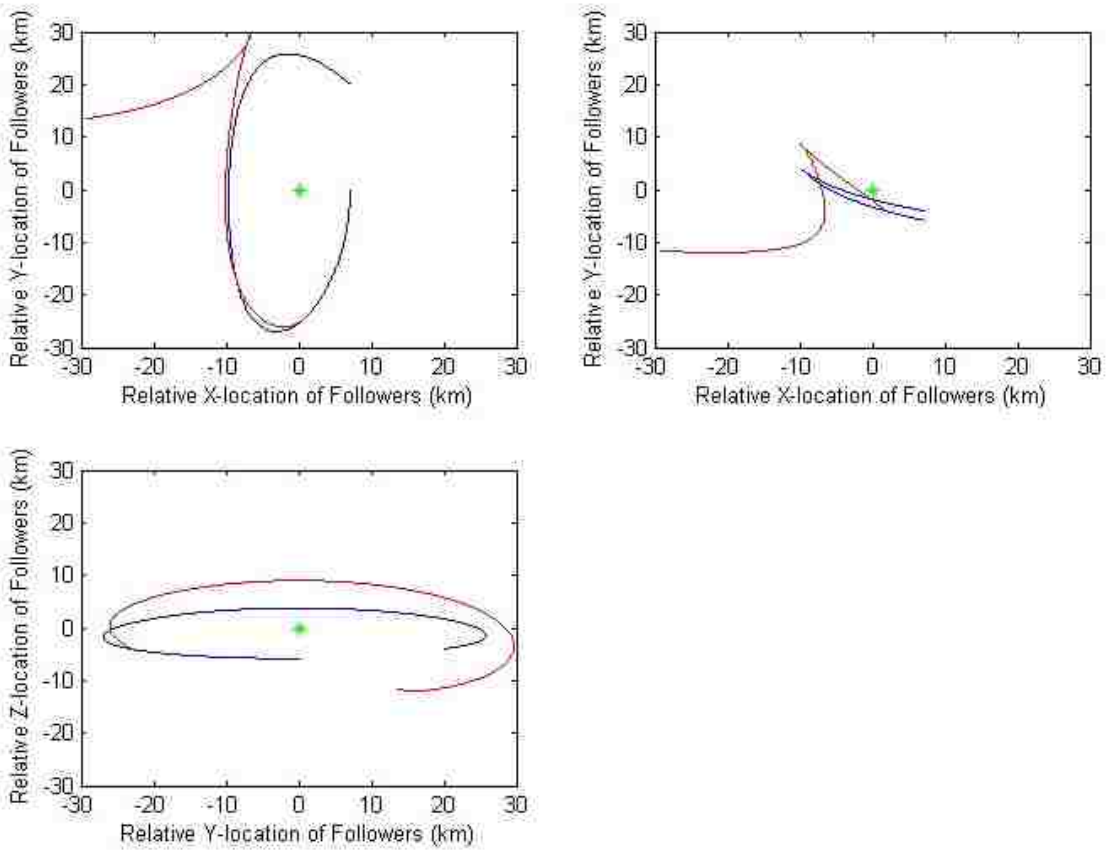

Figure 3.5. Alternate Differentially Corrected Halo Orbit

With these two methods failing to find a natural match to the reference follower spacecraft's trajectory, it was decided that any specific follower spacecraft would need to be individually controlled to maintain a reference halo orbit about a leader spacecraft if the starting position was varied along the reference follower's trajectory. Thus, it is unlikely that differential corrections will identify a natural (uncontrolled) solution in which the additional follower spacecraft would precisely follow the same trajectory as the reference follower solution. Instead, active control would need to be applied to the follower spacecraft to "force" their orbits to match the reference trajectory.

Due to the wide range of possibilities for placing a follower spacecraft on any sort of relative halo orbit with respect to a leader spacecraft on its own halo orbit, a parametric study to determine the possibility of any natural relative halo orbits was not performed. The methods used in this study could be implemented based on a set of mission requirements and initial conditions to determine the feasibility of a natural

relative halo orbit formation. The inputs required to determine the feasibility would be the initial positions of the follower spacecraft coupled with any mission requirements that govern the period of the halo orbits or their relative motion with respect to the leader spacecraft that would be pertinent to the mission.

3.2.3. Fixed Position Relative to Leader Spacecraft Orbit. The next formation type examined was locating the follower spacecraft in a fixed position relative to the leader spacecraft. This type of formation maintains a specific orientation relative to the leader spacecraft in the rotating frame (with respect to the two primaries) and is useful for satisfying scientific pointing requirements in the rotating frame (Sun, Earth, or Moon). The leader spacecraft's nominal orbit was considered known for purposes of this research. Since the follower's position is defined relative to the leader and the leader's trajectory is considered known, the follower's nominal or reference trajectory is also considered known at all times.

The given inputs for a fixed-position follower are a specified position relative to the leader spacecraft coupled with an error tolerance (as defined by scientific requirements) to the distance magnitude. In other words, the formation needs to maintain all of the relative position components with respect to each other in order to maintain the specific formation. The error tolerance on the distance magnitude generates an error "sphere" surrounding the follower spacecraft. In terms of the trajectory, this establishes an error corridor in which the follower spacecraft must remain at all times. As long as the follower spacecraft remains within the error corridor, it is deemed that the formation is being maintained.

Four cases were examined where the distance magnitude was the parameter arbitrarily varied at ten meters, one hundred meters, one kilometer and ten kilometers. For all cases, the error tolerance on the distance magnitude was kept at one centimeter and the initial relative velocities were set at zero. The value of one centimeter was used due to requirements for interferometry based on a NASA Goddard Spaceflight Center research announcement[44]. The initial states of the follower for the ten meter example are:

$$\begin{Bmatrix} x_o \\ y_o \\ z_o \end{Bmatrix} = \begin{Bmatrix} 5.7735 \\ 5.7735 \\ -5.7735 \end{Bmatrix} \text{ m}$$

$$\begin{Bmatrix} \dot{x}_o \\ \dot{y}_o \\ \dot{z}_o \end{Bmatrix} = \begin{Bmatrix} 0 \\ 0 \\ 0 \end{Bmatrix} \frac{\text{km}}{\text{s}}$$

These initial conditions were selected by using a similar method as the relative halo orbit formation (Section 3.2.1) of determining convenient neighborhoods (fourteen points) for a particular type of formation. These fourteen points differ with the assumption of one position being zero was not used. Table 3.2 contains the fourteen initial cases examined for the ten kilometer formation size. For the case of a specified relative position that must be maintained, a positive x-position, positive y-position and negative z-position yielded the best (maintained its relative position for the longest period of time) natural starting position for a follower spacecraft (highlighted). Table 3.3 contains data illustrating the relative distance magnitudes (km) of each spacecraft after 90 and 150 days and shows why the second formation geometry was chosen.

Table 3.2. Initial Coordinates of Follower Spacecraft

	X (km)	Y (km)	Z (km)
1	5.7735	5.7735	5.7735
2	**5.7735**	**5.7735**	**-5.7735**
3	5.7735	-5.7735	5.7735
4	5.7735	-5.7735	-5.7735
5	-5.7735	5.7735	5.7735
6	-5.7735	5.7735	-5.7735
7	-5.7735	-5.7735	5.7735
8	-5.7735	-5.7735	-5.7735
9	10.000	0	0
10	-10.000	0	0
11	0	10.000	0
12	0	-10.000	0
13	0	0	10.000
14	0	0	-10.000

Table 3.3. Relative Distance Magnitude (km) of Follower Drift

	90 days	150 days
1	128.365	1535.521
2	**9.3812**	**21.201**
3	207.537	2592.871
4	153.512	1851.772
5	232.711	2912.179
6	207.554	2595.302
7	153.529	1853.020
8	128.377	1536.421
9	312.433	3847.707
10	312.481	3853.468
11	68.996	916.224
12	68.995	916.512
13	23.635	274.081
14	23.635	274.066

The initial attempts at maintaining the fixed relative position formation were accomplished using the same differential corrections technique described above where the initial velocities are changed in order to target a specific end state (a specific position for this case). For all cases, the initial uncorrected relative velocities were all zero. In other words, the follower spacecraft were placed in their relative positions with zero relative velocities. All the formations followed the same pattern of each starting location having components such that the x, y-values were each positive and the z-value negative, due to the information from Table 3.3.

The goal was to maximize the time spent in the error corridor while monitoring the $\Delta\mathbf{V}$ requirements. The follower's trajectory is also continuously checked to ensure that at no point leading up to the defined end time does the follower spacecraft violate the error corridor.

The calculation of the end time state was a two-step process. Originally, the spacecraft trajectory was propagated until it violated the error corridor. It was determined that in any real situation, allowing the follower spacecraft to drift to the maximum allowable error could be risky. Thus, the defined end state was changed. Instead, for the cases where the time in the error corridor was maximized, rather than take the end time as the point where the spacecraft violates the error corridor, the end time was defined by the

moment when the spacecraft passes nearest the reference orbit after having been propagated for some minimum time (arbitrarily defined as ten minutes). In other words, rather than allow the follower spacecraft to travel all the way to the time at which it violates the error corridor, it was stopped at the moment it passed closest to the reference trajectory.

The new definition for the end time led to an end state that was very near the follower reference orbit and on the same trajectory that maximized the time spent in the error corridor without propagating the spacecraft to the limit of the error bound. Multiple segments were then propagated to define an overall trajectory with $\Delta\mathbf{V}$s at the beginning of every new segment to maximize the time spent in the error corridor for that specific segment.

Figures 3.6-3.9 represent the final (of five) segment propagations for four different formation sizes. Each formation had the same relative starting location for the follower spacecraft with only the distance magnitude changed. The red lines represent the maximum error bound (one centimeter) on either side of the nominal trajectory. The green line represents the reference orbit trajectory. The blue line defines the actual trajectory of the follower spacecraft over the particular segment. It should be noted that it is a combination of all three position components that define an overall distance magnitude. Additionally, the follower spacecraft was to remain within one centimeter of a fixed position, not just maintain a fixed distance from the leader spacecraft.

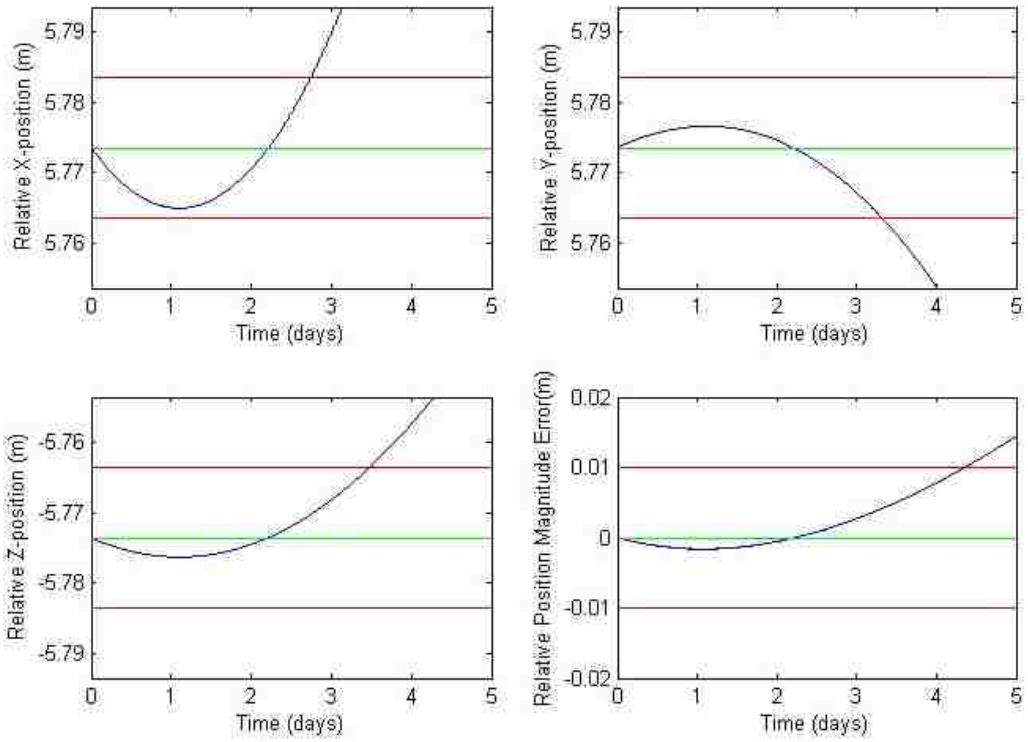

Figure 3.6. 10 m Formation Size – 1 cm Error Bound

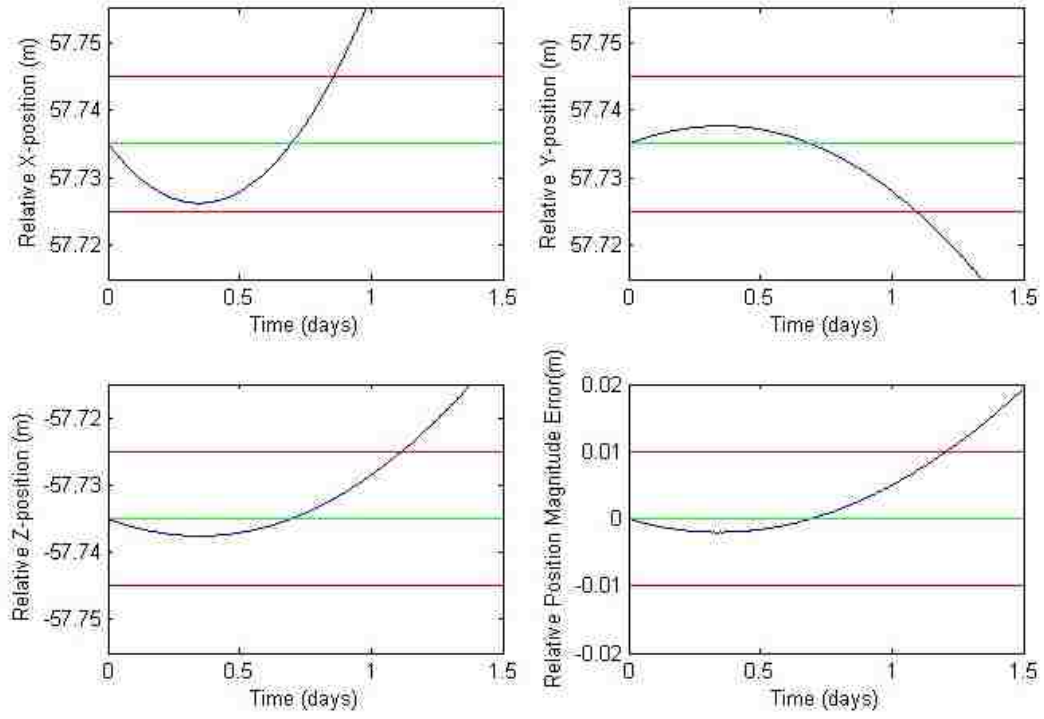

Figure 3.7. 100 m Formation Size – 1 cm Error Bound

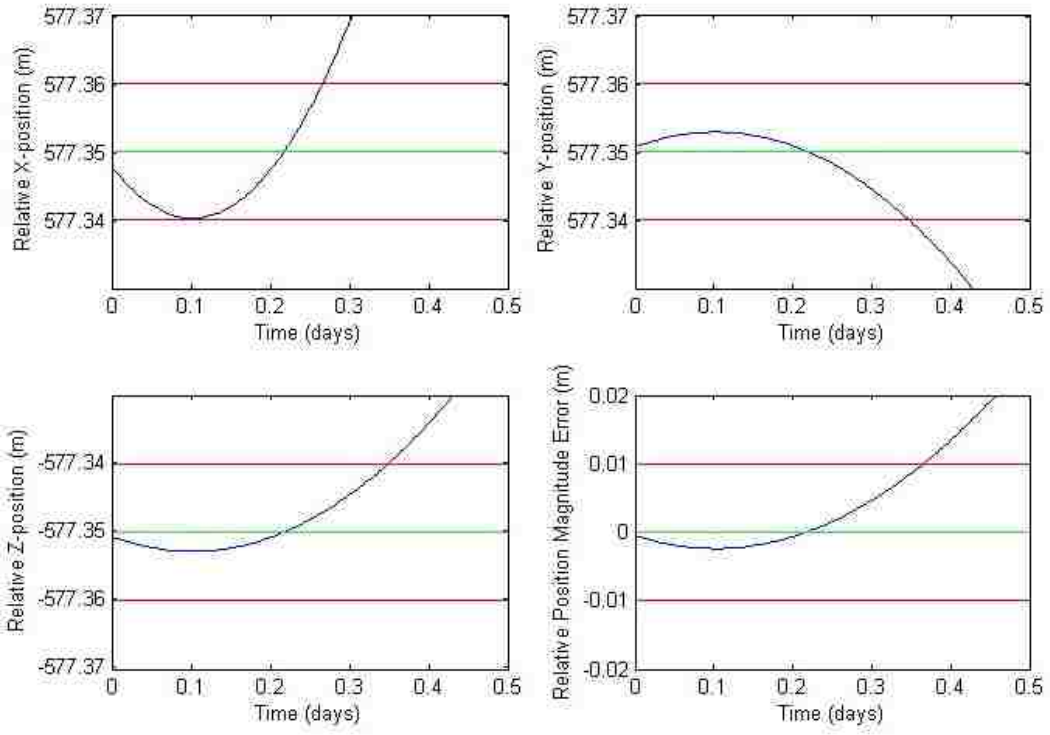

Figure 3.8. 1 km Formation Size – 1 cm Error Bound

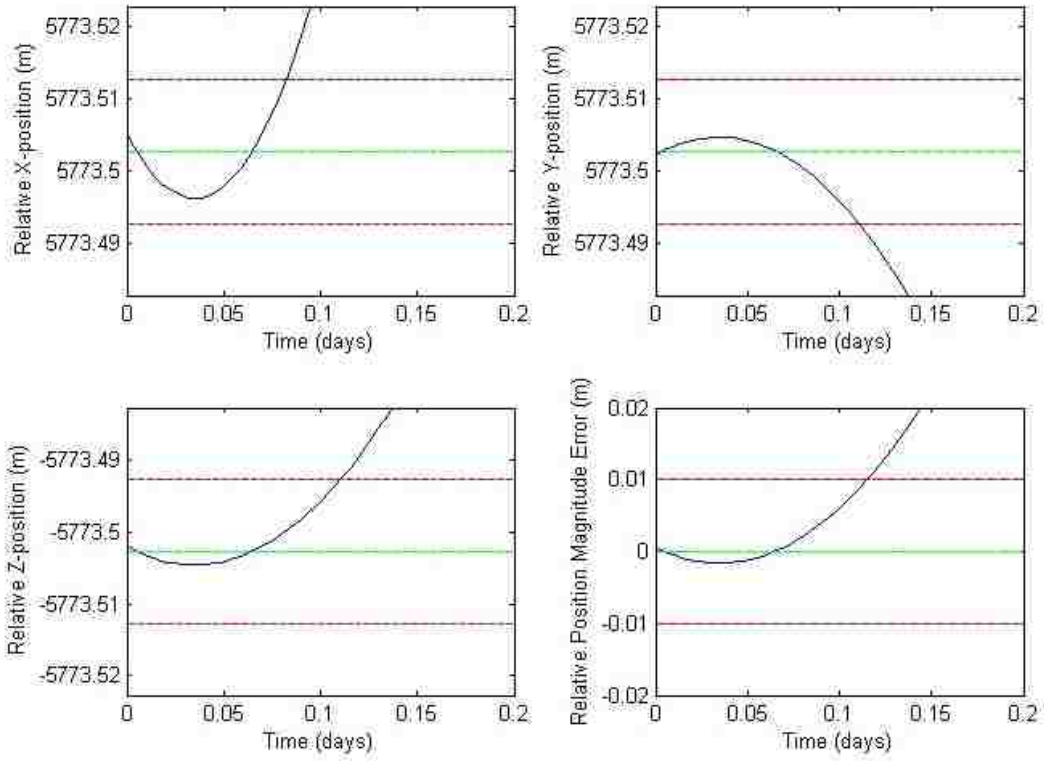

Figure 3.9. 10 km Formation Size – 1 cm Error Bound

Table 3.4 shows the time spent (hours) within the error corridor for each segment of a given formation size. Each formation was propagated for a total of five segments, regardless of the segment length. Five segments were computed because they supplied sufficient information to establish a qualitative trend for each formation. Any number of segments could be linked to construct a trajectory of any desired duration for any formation size. The maximum error distance allowed for all formation distances was one centimeter but other error sizes could be used based on the mission requirements.

As can be seen in Table 3.4, time spent in the error corridor is approximately inversely proportional to the formation size. As the formation size increases, sensitivities in the motion become greater causing the follower spacecraft to more quickly drift away from its reference orbit. Time spent in the error corridor is of interest for possible scientific requirements of long viewing times. The other points of interest are the $\Delta\mathbf{V}$ requirements to maintain the formation. The $\Delta\mathbf{V}$ requirements will directly influence the viability and longevity of a particular mission.

Table 3.4. Time in Error Corridor (Hours) for Four Formation Sizes

Formation Size	Segment 1	Segment 2	Segment 3	Segment 4	Segment 5
10 m	52.5167	57.7167	52.8833	53.0000	53.0500
100 m	16.5333	11.6667	16.9333	17.0333	16.6500
1 km	5.25000	5.75000	5.26667	5.25000	5.25000
10 km	1.68333	1.83333	1.48333	1.50000	1.48333

Table 3.5 shows the $\Delta\mathbf{V}$ required at the end of each segment to correct the follower spacecraft to maintain its trajectory within the error corridor (without venturing too close to the error bound) for the following segment. It was assumed that the initial $\Delta\mathbf{V}$ was zero, so that the follower spacecraft starts out with the exact initial states required to maximize the time spent in the error corridor. All of the $\Delta\mathbf{V}$s are between $3.9\text{x}10^{-7}$ and $1.5\text{x}10^{-5}$ m/s, well within the ESA's microthruster capability.

Table 3.5. $\Delta\mathbf{V}$ Magnitudes (m/s) for Four Formation Sizes

Formation Size	$\Delta\mathbf{V}_1$ (m/s)	$\Delta\mathbf{V}_2$ (m/s)	$\Delta\mathbf{V}_3$ (m/s)	$\Delta\mathbf{V}_4$ (m/s)
10 m	4.495×10^{-7}	4.053×10^{-7}	4.001×10^{-7}	3.985×10^{-7}
100 m	1.418×10^{-6}	1.339×10^{-6}	1.320×10^{-6}	1.270×10^{-6}
1 km	4.506×10^{-6}	4.070×10^{-6}	4.010×10^{-6}	4.004×10^{-6}
10 km	1.452×10^{-5}	1.121×10^{-5}	1.096×10^{-5}	1.090×10^{-5}

As the formation size increases, the follower spacecraft will drift more quickly away from the reference orbit. Coupled with this, the $\Delta\mathbf{V}$ required to correct the follower spacecraft so that it stays within the error corridor also increases. The follower spacecraft must make larger and more frequent $\Delta\mathbf{V}$s to remain in its nominal position to maintain the formation.

As stated in reference 33, ESA describes hardware with the ability to create thrust in the range of 0.1-150 micronewtons with a precision of ±0.1 micronewtons. The time response of the propulsive system is on the order of 190 milliseconds. Given a spacecraft mass of around one hundred kilograms, that translates to a $\Delta\mathbf{V}$ on the order of 1×10^{-9} m/s, well within the minimum required by the one centimeter error tolerance for the above formations.

Additional follower spacecraft in their own fixed relative positions could be added to the formation. Care would need to be taken to ensure that the formation as a whole exploits the natural dynamics of the system. Careful examination of the "neighborhoods" that lend themselves toward natural formations would need to take place to ensure the entire formation (or most of it) takes advantage of the natural dynamics.

3.2.4. Paraboloid Formation. The next formation type examined was with a follower spacecraft constrained to the surface of a paraboloid. The NASA Goddard Spaceflight Center issued a research announcement calling for studies to be conducted in the area of aspherical formations near libration points[44]. The ultimate goal of the research was to fly a formation of spacecraft (on the order of twenty spacecraft) on a paraboloid surface to form a distributed Fizeau interferometer for a mission such as the Stellar Imager (mentioned earlier) with a mission life near twelve years. The primary

specification used from this announcement was the one centimeter error bound on the formation relative positions. Additional specifications were outlined in the research announcement such as length of formation pointing ("stare" in an inertially fixed direction for up to a month), formation rotation (must rotate about the line of sight to the target at least once per week) and a maneuver mode (line of sight of the aperture must slew on the order of twenty degrees per day to acquire a new science target) but are not in the present scope of this research.

For this study, the leader spacecraft was assumed to be located at the vertex of the paraboloid with the follower spacecraft fixed at some "altitude" above the follower spacecraft along the surface of the paraboloid. Figure 3.10 illustrates the paraboloid and the follower's error "torus."

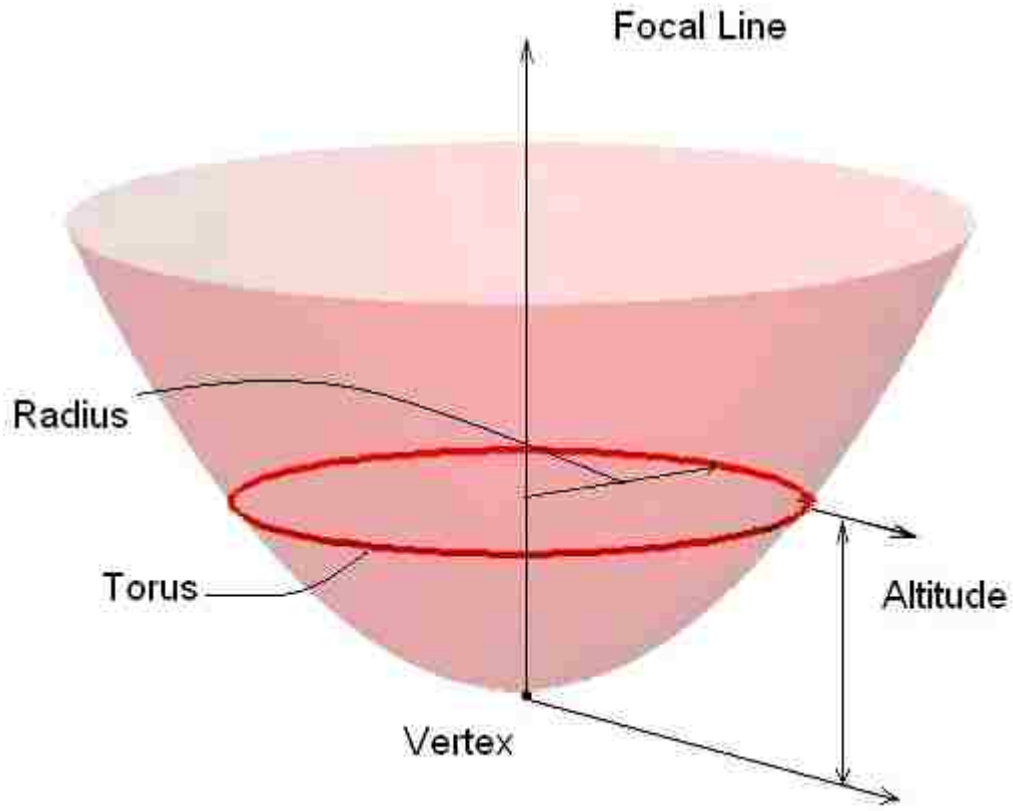

Figure 3.10. Example Paraboloid[43] with Error Torus

The paraboloid itself could vary considerably in its size and overall shape and would typically be defined by the science requirements of a particular mission. For the

purposes of this research, the paraboloid was assumed to take the shape where the altitude was equal to the radius for the initial case. Other follower spacecraft could then be added to the paraboloid surface at any location. It should be noted that the follower spacecraft were free to move around anywhere within the error torus. An additional constraint would need to be applied to guarantee that any follower spacecraft positioned at the same (or close) relative altitude would not collide, especially during a reorientation of the formation. The process of reorienting the entire formation was not investigated in this study.

Two different scenarios were examined for the paraboloid formation. The first example was treated much like the fixed-position formation discussed in the previous section except that a different constraint is applied to the follower spacecraft. The formation as a whole maintained the same orientation relative to the rotating frame, useful for observation of the two primaries or other objects in the rotating frame. The second example required the formation to maintain a fixed orientation in the inertial frame, useful for observation of inertially fixed objects. The second example is discussed later in this section.

3.2.5. Paraboloid Formation in Rotating Frame For the first example, defining the error torus was the first step in the process. Based on the pointing of the formation, the leader spacecraft was placed at the vertex of the paraboloid and the next step was to define the shape and size of the paraboloid. Based on the chosen size of the paraboloid, an altitude and radius were defined for the follower. The next step was to add a follower spacecraft to the paraboloid at some defined altitude. With the follower spacecraft's initial position defined by the paraboloid's pointing and the spacecraft's altitude, the allowable error torus was defined for that particular altitude. The follower spacecraft was then constrained to stay within the error torus. This was accomplished by maintaining an error tolerance (one centimeter) on the altitude and an error tolerance (one centimeter) on the distance magnitude. If either constraint was violated at any time, the follower spacecraft was considered outside the error torus.

By mimicking the fixed-position formation, the calculation of the end time state for the paraboloid formation used the same two-step process. The follower spacecraft was

given the same initial conditions as the fixed position case. The following show the initial conditions for the ten meter formation size:

$$\begin{Bmatrix} x_o \\ y_o \\ z_o \end{Bmatrix} = \begin{Bmatrix} 5.7735 \\ 5.7735 \\ -5.7735 \end{Bmatrix} \text{ m}$$

$$\begin{Bmatrix} \dot{x}_o \\ \dot{y}_o \\ \dot{z}_o \end{Bmatrix} = \begin{Bmatrix} 0 \\ 0 \\ 0 \end{Bmatrix} \frac{\text{km}}{\text{s}}$$

The follower spacecraft was propagated until it violated the error torus. Rather than take the end time as the point where the spacecraft violates the error torus, the end time was defined by the moment when the spacecraft passes nearest the reference orbit after having been propagated for some minimum time (arbitrarily defined as ten minutes), as was done in the fixed-position formation case. This process helps ensure that the follower spacecraft does not approach the error torus bounds with significant velocities that could continue to take it out of the error torus.

The above definition of the end-time led to an end-state that was very near the follower reference orbit (located anywhere around the paraboloid on the torus but at the fixed altitude) and on the same trajectory that maximized the time spent in the error torus without propagating the spacecraft all the way to the limit of the error torus. Multiple segments were then propagated to define an overall trajectory with $\Delta\mathbf{V}$s at the beginning of every new segment to maximize the time spent in the error corridor for that specific segment. A total of five segments were propagated.

Tables 3.6-3.8 represents an example of the time spent in the error torus for various formation sizes and orientations with a fixed error tolerance (one centimeter) over five different segments. Three different orientations for the paraboloid were explored. For simplicity, the three cases had the formation pointing along one of the rotating axes (x, y, z-axis). As the formation size increases while maintaining a constant error tolerance, the time spent in the error torus decreases, as expected considering the relative similarity of the paraboloid formation to the fixed-position formation. Additionally, the orientation of

the formation also has implications on the natural dynamics. The y-axis and z-axis orientations were comparable, but the x-axis orientation tended to only remain in the error torus half as long as the other two orientations. Additional orientations would need to be explored based on mission pointing requirements to determine natural formations that also satisfy time spent in the error torus requirements.

Table 3.6. Time Spent (Hours) in Error Torus for Various Formation Sizes and Formation Pointing Along the Rotating X-Axis

Formation Size	Segment 1	Segment 2	Segment 3	Segment 4	Segment 5
10 m	54.7500	59.6667	49.6667	50.6667	51.1667
100 m	17.3333	18.9167	15.5833	15.5833	15.6667
1 km	5.5000	5.91667	4.91667	5.0000	4.91667

Table 3.7. Time Spent (Hours) in Error Torus for Various Formation Sizes and Formation Pointing Along the Rotating Y-Axis

Formation Size	Segment 1	Segment 2	Segment 3	Segment 4	Segment 5
10 m	99.2500	98.6667	95.6667	100.333	95.4167
100 m	32.0833	34.6667	31.6667	32.0000	34.4167
1 km	10.2500	11.1667	10.16667	10.0000	10.0000

Table 3.8. Time Spent (Hours) in Error Torus for Various Formation Sizes and Formation Pointing Along the Rotating Z-Axis

Formation Size	Segment 1	Segment 2	Segment 3	Segment 4	Segment 5
10 m	93.6667	92.5000	89.0833	87.6667	86.4167
100 m	32.2500	35.1667	31.9167	31.8333	31.6667
1 km	10.2500	11.1667	10.1667	10.1667	10.1667

Tables 3.9-3.11 illustrate the $\Delta\mathbf{V}$ magnitudes for five segments (the initial point on the first segment is assumed to require no $\Delta\mathbf{V}$). Considering the wide range of possibilities for formation sizes and orientation, a more exhaustive study would need to be performed for specific mission applications. The y-axis and z-axis cases were

comparable once again while the x-axis orientation required roughly half the $\Delta\mathbf{V}$ requirements. Comparing the two sets of tables it can be seen that the x-axis orientation is not considerably more efficient than the other two cases, as it requires smaller but more frequent $\Delta\mathbf{V}$s to maintain the formation. Table 3.11 below contains the average $\Delta\mathbf{V}$s per day for each formation size and orientation. For the cases shown here, the x-axis orientation requires nearly half the $\Delta\mathbf{V}$ magnitudes but only lasts approximately half as long in the error torus.

Table 3.9. $\Delta\mathbf{V}$ Magnitude (m/s) for Formation Size and Formation Pointing on the Rotating X-Axis

Formation Size	$\Delta\mathbf{V}_1$ (m/s)	$\Delta\mathbf{V}_2$ (m/s)	$\Delta\mathbf{V}_3$ (m/s)	$\Delta\mathbf{V}_4$ (m/s)
10 m	4.672×10^{-7}	3.665×10^{-7}	3.656×10^{-7}	3.659×10^{-7}
100 m	1.488×10^{-6}	1.168×10^{-6}	1.139×10^{-6}	1.131×10^{-6}
1 km	4.697×10^{-6}	3.639×10^{-6}	$3.697x\ 10^{-6}$	3.572×10^{-6}

Table 3.10. $\Delta\mathbf{V}$ Magnitude (m/s) for Formation Size and Formation Pointing on the Rotating Y-Axis

Formation Size	$\Delta\mathbf{V}_1$ (m/s)	$\Delta\mathbf{V}_2$ (m/s)	$\Delta\mathbf{V}_3$ (m/s)	$\Delta\mathbf{V}_4$ (m/s)
10 m	8.590×10^{-7}	6.795×10^{-7}	7.923×10^{-7}	$7.433x\ 10^{-7}$
100 m	2.721×10^{-6}	2.694×10^{-6}	2.734×10^{-6}	2.722×10^{-6}
1 km	8.738×10^{-6}	7.891×10^{-6}	$7.670x\ 10^{-6}$	7.603×10^{-6}

Table 3.11. ΔV Magnitude (m/s) for Formation Size and Formation Pointing on the Rotating Z-Axis

Formation Size	$\Delta\mathbf{V}_1$ (m/s)	$\Delta\mathbf{V}_2$ (m/s)	$\Delta\mathbf{V}_3$ (m/s)	$\Delta\mathbf{V}_4$ (m/s)
10 m	7.079×10^{-7}	6.241×10^{-7}	6.322×10^{-7}	6.210×10^{-7}
100 m	2.747×10^{-6}	2.461×10^{-6}	2.421×10^{-6}	2.399×10^{-6}
1 km	8.744×10^{-6}	7.832×10^{-6}	$7.770x\ 10^{-6}$	7.727×10^{-6}

Table 3.12 contains the $\Delta\mathbf{V}$ magnitudes for each formation size and orientation. The ΔV magnitudes were generated by taking the average time spent in the error corridor over the five segments and determining the number of segments in a given day. The next

step was to determine the average $\Delta\mathbf{V}$ magnitude for each segment. This average $\Delta\mathbf{V}$ magnitude was then multiplied by the number of segments in a day to determine the total amount of $\Delta\mathbf{V}$ expended for each formation size and orientation. A general trend emerges that as the size of the orientation increases by an order of magnitude, the $\Delta\mathbf{V}$ requirement to maintain that formation also increases by an order of magnitude. Also, each of the orientations is roughly equivalent in their $\Delta\mathbf{V}$ requirement over a day but the number of $\Delta\mathbf{V}$s performed in a given day is not constant. The orientation pointing in the x-direction requires nearly double the number of maneuvers than the y-orientation and z-orientations as can be seen by comparing the time spent in the error corridor contained in Tables 3.8-3.10.

Table 3.12. $\Delta\mathbf{V}$ Magnitude (m/s) per Day for Each Formation and Orientation

Formation Size	X-Pointing	Y-Pointing	Z-Pointing
10 m	1.766×10^{-7}	1.885×10^{-7}	1.726×10^{-7}
100 m	1.779×10^{-6}	1.979×10^{-6}	1.848×10^{-6}
1 km	1.783×10^{-5}	1.855×10^{-5}	1.853×10^{-5}

Figures 3.11-3.19 show the final (of five) segment propagation for the three different formation sizes (10 m, 100 m, 1 km) and the three different orientations (x, y, z-axis). Each formation had the same relative starting location for the follower spacecraft with the distance magnitude changed (ten meters and one kilometer). The red lines represent the maximum error bound (one centimeter) on either side of the nominal trajectory. The green line represents the reference orbit trajectory. The blue line defines the actual trajectory of the follower over the particular segment.

The follower spacecraft was allowed to move within the error torus. It should be noted that it is a combination of all three position components that define an overall relative distance magnitude. The actual constraints applied to the follower spacecraft were that the overall relative distance magnitude not vary by more than one centimeter and that, based on the orientation, the altitude of the follower spacecraft not vary by more than one centimeter. In other words, the spacecraft was free to change its relative position along either of the two axes that were not defined by the altitude while maintaining a

fixed overall relative distance magnitude. As stated in Section 3.2.3, the $\Delta\mathbf{V}$ magnitudes are well within ESA's microthruster's capabilities.

Additional follower spacecraft could be added to the paraboloid formation at different altitudes. Multiple spacecraft could be added at the same altitude but particular care would need to be taken to ensure that the spacecraft would never collide. An additional constraint would need to be applied to the follower spacecraft to ensure they remain on a particular portion of the paraboloid at a given altitude.

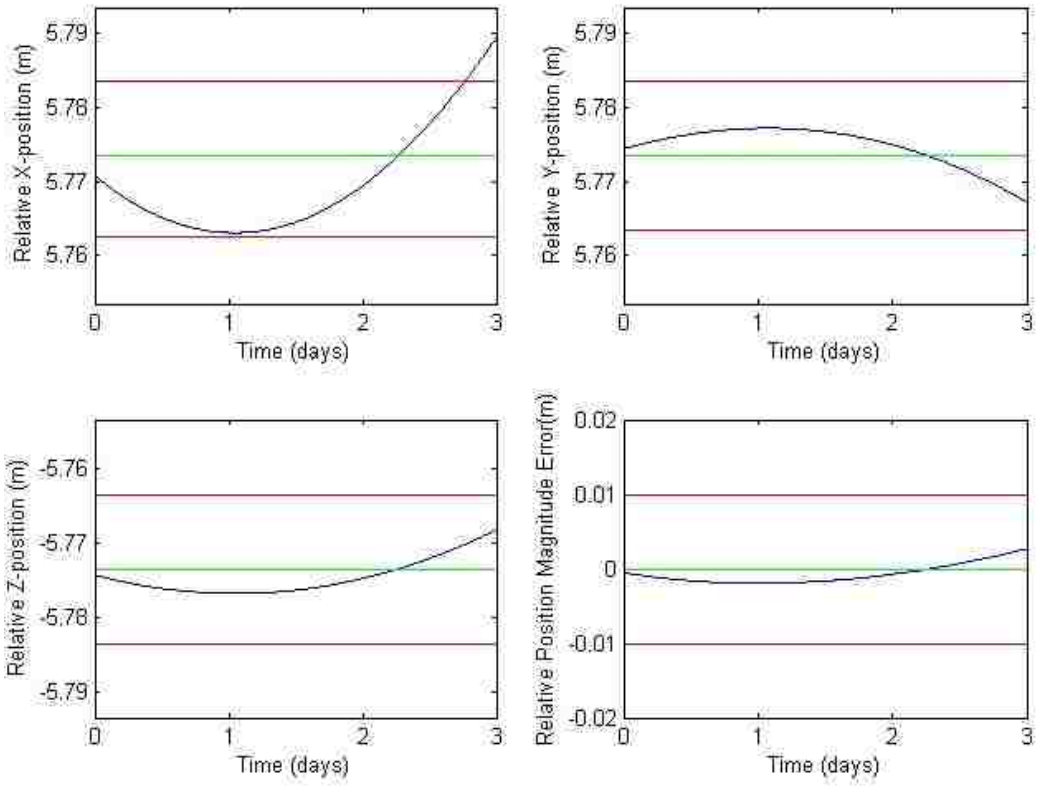

Figure 3.11. 10 m Formation with Formation Pointing along the Rotating X-Axis

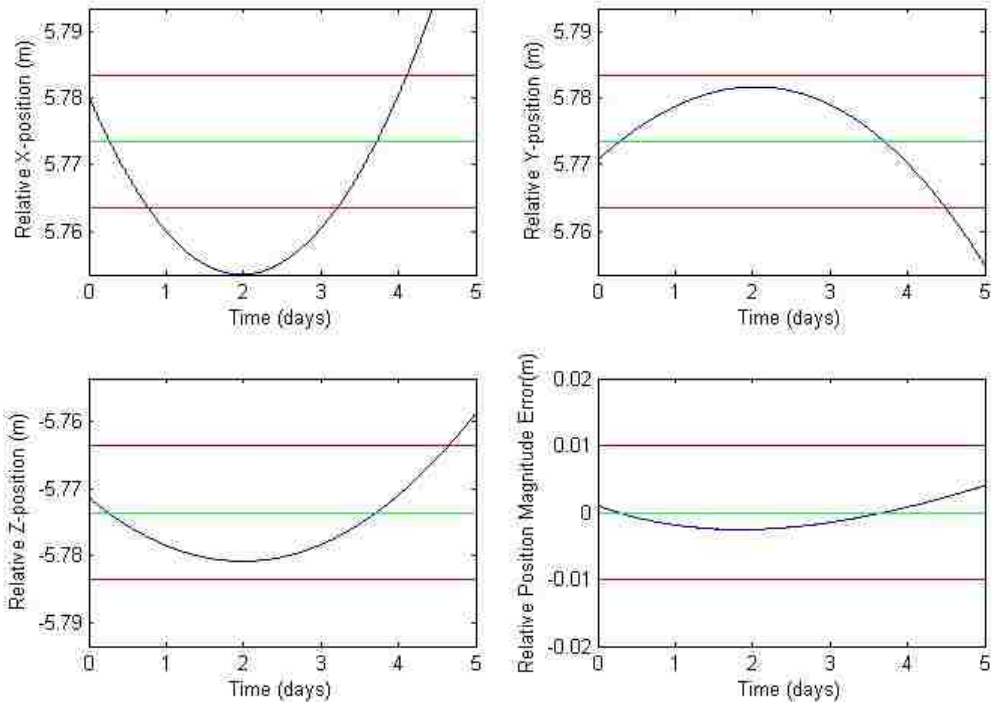

Figure 3.12. 10 m Formation with Formation Pointing along the Rotating Y-Axis

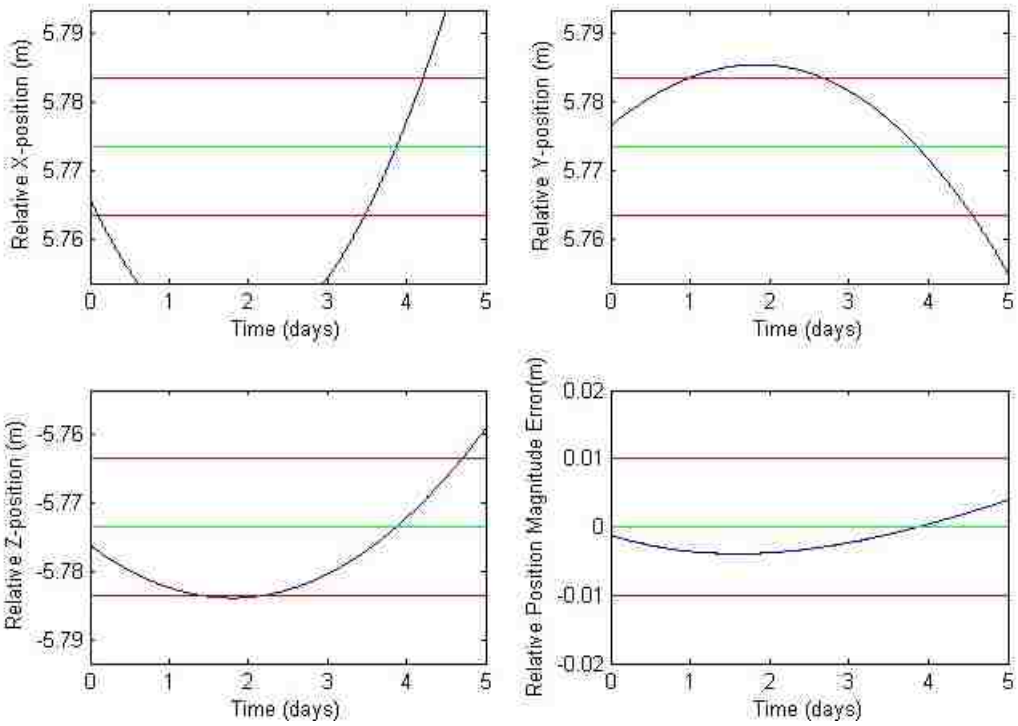

Figure 3.13. 10 m Formation with Formation Pointing along the Rotating Z-Axis

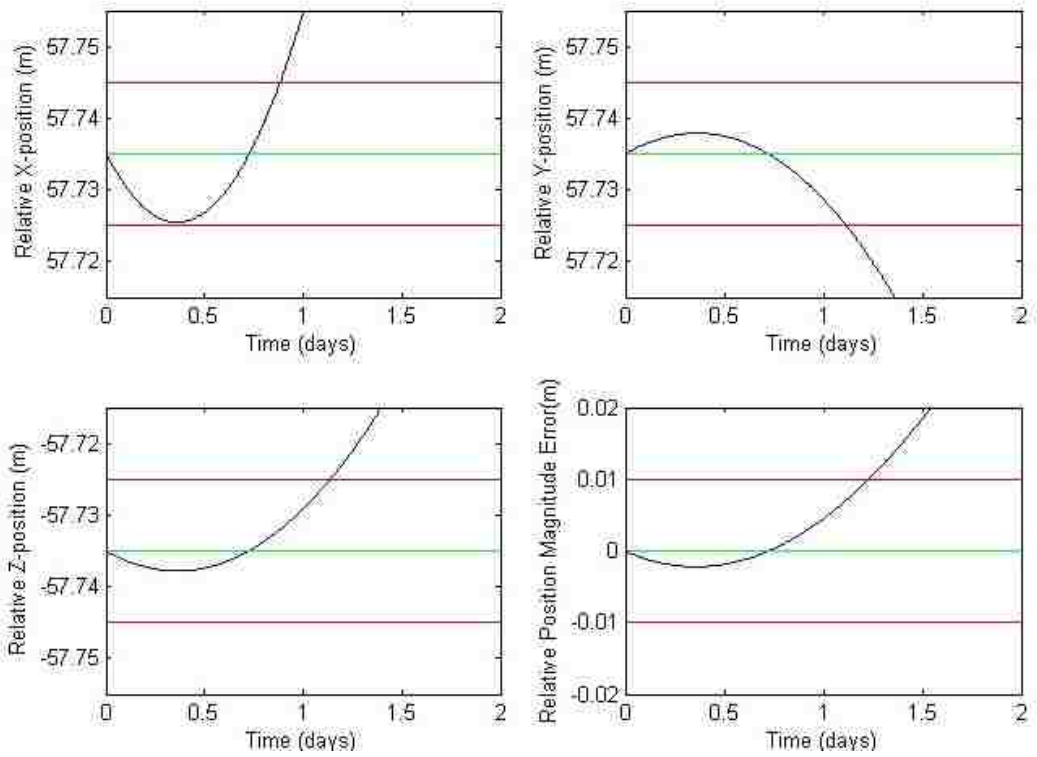

Figure 3.14. 100 m Formation with Formation Pointing along the Rotating X-Axis

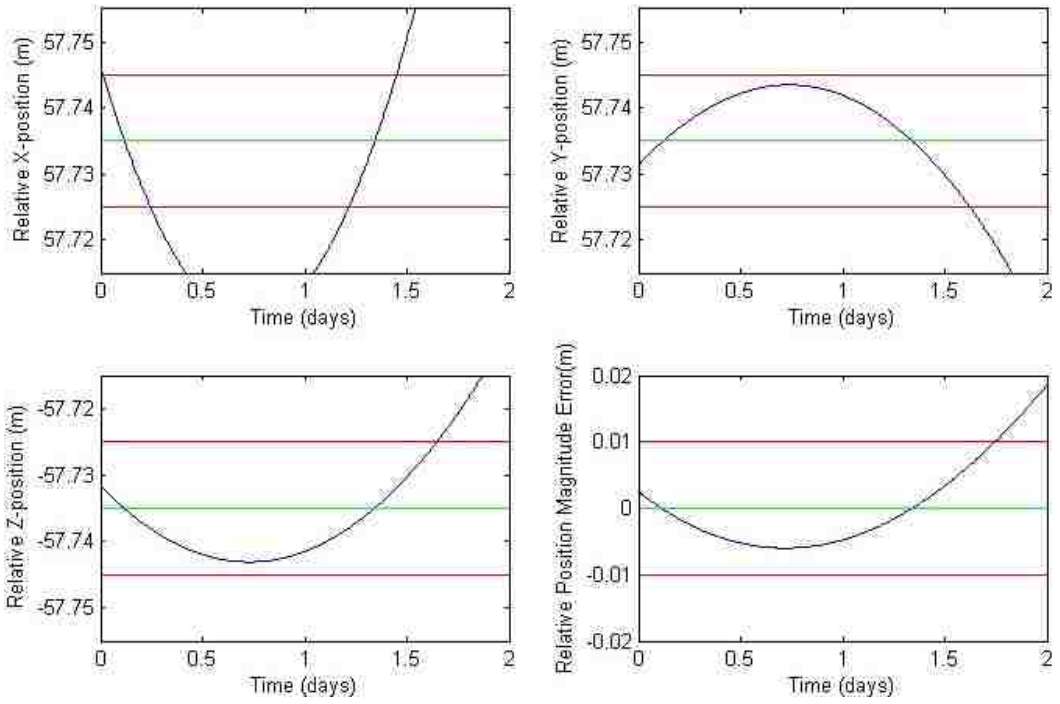

Figure 3.15. 100 m Formation with Formation Pointing along the Rotating Y-Axis

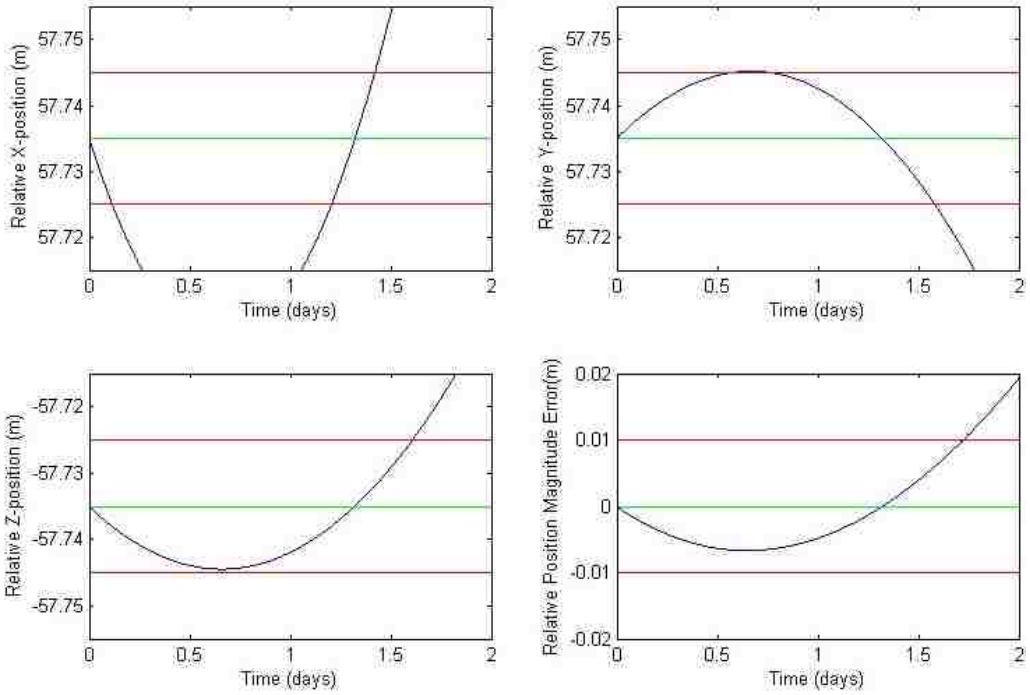

Figure 3.16. 100 m Formation with Formation Pointing along the Rotating Z-Axis

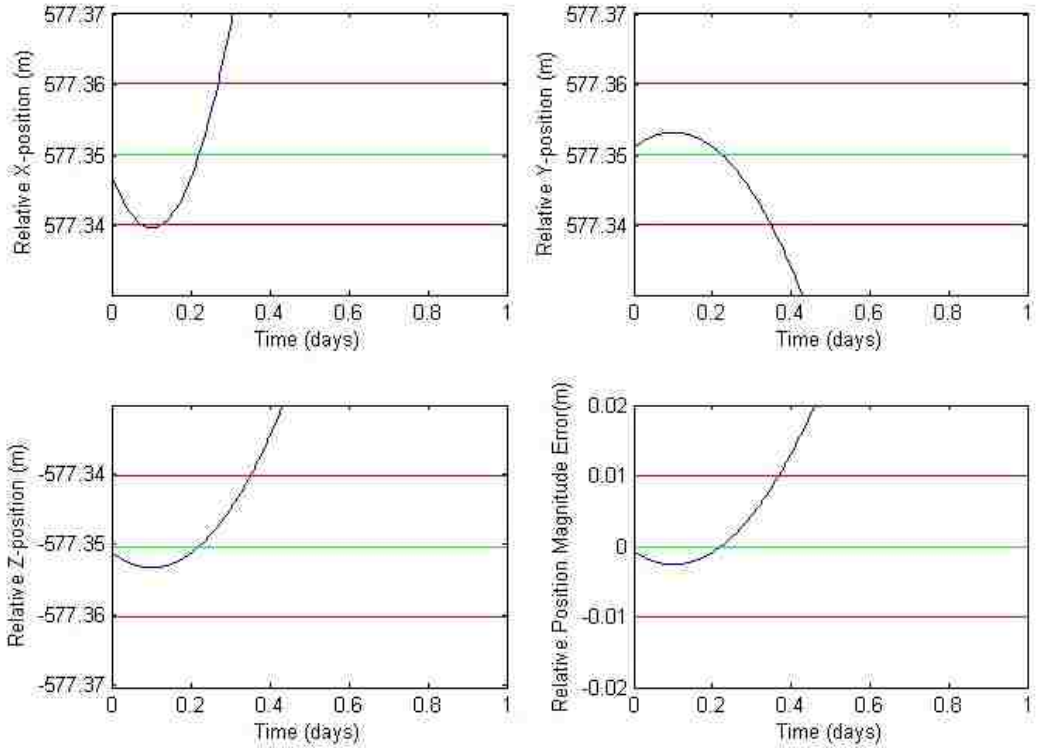

Figure 3.17. 1 km Formation with Formation Pointing along the Rotating X-Axis

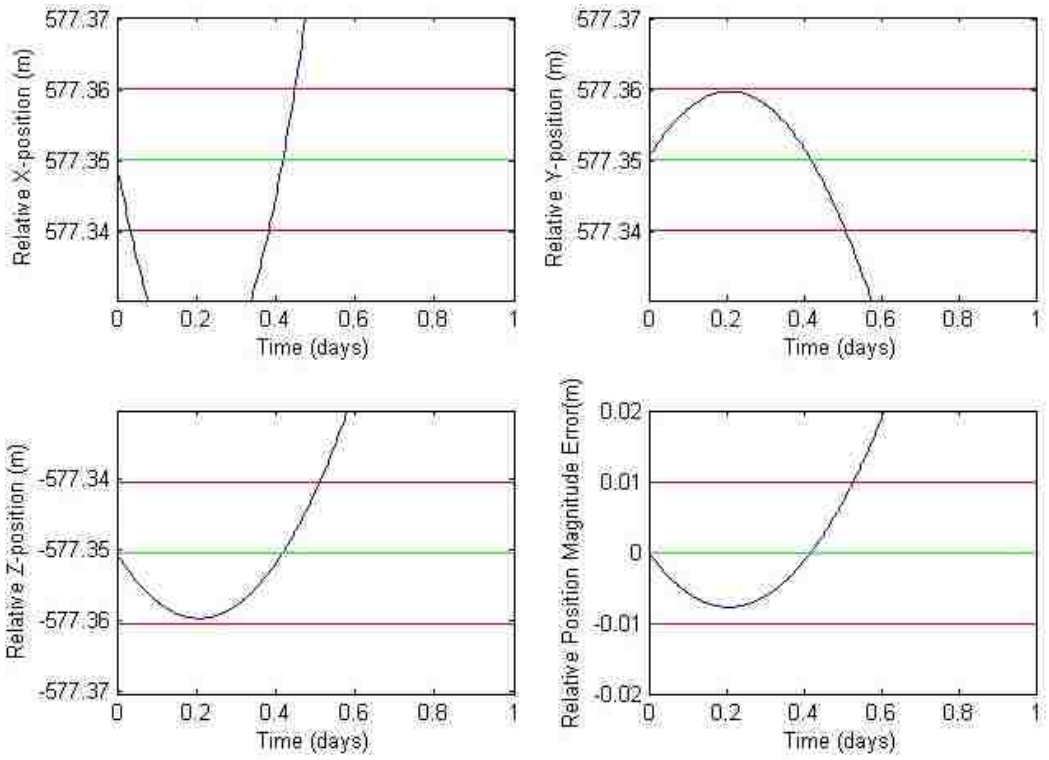

Figure 3.18. 1 km Formation with Formation Pointing along the Rotating Y-Axis

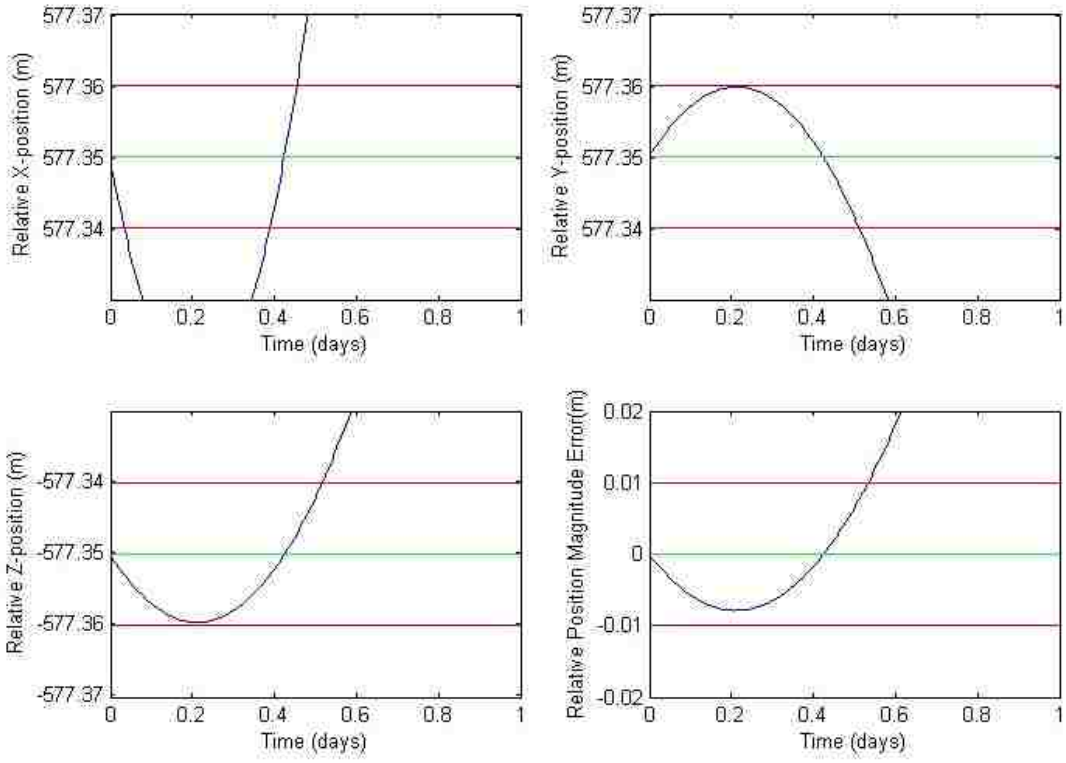

Figure 3.19. 1 km Formation with Formation Pointing along the Rotating Z-Axis

3.2.6. Paraboloid Formation in Inertial Frame The first paraboloid formation example maintained a formation relative to the rotating frame of the two primaries. The second paraboloid formation described in this section maintains the same formation orientation with respect to the *inertial* frame. Because the dynamics of three body system are expressed using a rotating frame, generating an inertially oriented formation becomes more challenging. The rotating frame angular rate is slightly more than one degree per day (360 degrees in 365.24 days). Because of this relatively small angular rate, large differences between the maintenance of the two formation types were not expected. Otherwise, this second formation type used the same initial conditions and processes as the first example.

Three different orientations were examined for the inertially fixed paraboloid formation. Similar to the first paraboloid formation example, the straightforward cases of pointing the formation along the inertially fixed axes were explored. The inertially fixed axis was defined as being equal to the rotating frame axis system at the initial starting time. In other words, at time equal to zero, the x-axes of the inertial frame and rotating frame are (arbitrarily) lined up with each other. For any time greater than zero, the rotating frame will begin to rotate while the inertially fixed axis system remains stationary. By definition of both frames, the z-axes are coincident at all times. Thus, the paraboloid formation z-axis pointing cases are the same for both rotating and inertial types. The direction cosine matrix (seen below) involved a rotation about the z-axis to align the x-axes. Since the z-axis did not change and any change in the angle due to the Earth's orbit about the Sun was safely ignored (due to the vast distances involved, this was a good assumption), only one rotation was required to maintain the orientation of the formation with respect to the inertial frame.

$$\begin{bmatrix} \cos(\theta) & \sin(\theta) & 0 \\ -\sin(\theta) & \cos(\theta) & 0 \\ 0 & 0 & 1 \end{bmatrix}$$

The angle, θ, was defined based on multiplying the time by the angular rate (360 degrees every 365.24 days). This angle was recalculated at every time step. The constraints that

the follower spacecraft maintain the same relative position was also updated at every time step. Thus, the follower spacecraft's nominal trajectory and error torus were defined.

Similar to the first paraboloid formation example, Tables 3.13-3.15 represents an example of the time spent in the error torus for various formation sizes and orientations with a fixed error tolerance (one centimeter) over five different segments.

Table 3.13. Time Spent (Hours) in Error Torus for Various Formation Sizes and Formation Pointing Along the Inertial X-Axis

Formation Size	Segment 1	Segment 2	Segment 3	Segment 4	Segment 5
10 m	54.0833	51.1667	50.6667	49.6667	50.1667
100 m	17.4167	18.5000	17.6667	16.1667	16.5833
1 km	6.2500	5.91667	4.66667	6.00000	4.58333

Table 3.14. Time Spent (Hours) in Error Torus for Various Formation Sizes and Formation Pointing Along the Inertial Y-Axis

Formation Size	Segment 1	Segment 2	Segment 3	Segment 4	Segment 5
10 m	97.4166	94.6667	97.6667	98.5000	95.4167
100 m	31.9167	33.6667	32.0000	31.4167	34.9167
1 km	10.0000	10.6667	10.2500	11.1667	9.91667

Table 3.15. Time Spent (Hours) in Error Torus for Various Formation Sizes and Formation Pointing Along the Inertial Z-Axis

Formation Size	Segment 1	Segment 2	Segment 3	Segment 4	Segment 5
10 m	93.6667	92.5000	89.0833	87.6667	86.4167
100 m	32.2500	35.1667	31.9167	31.8333	31.6667
1 km	10.2500	11.1667	10.1667	10.1667	10.1667

Tables 3.16-3.18 illustrate the $\Delta\mathbf{V}$ magnitudes for five segments (the starting location on the first segment is assumed to require no $\Delta\mathbf{V}$). The y-axis and z-axis cases were comparable once again while the x-axis orientation required roughly half the $\Delta\mathbf{V}$ requirements. Comparing the two sets of tables it can be seen that the x-axis orientation is not considerably more efficient than the other two cases, as it requires smaller but more frequent $\Delta\mathbf{V}$s to maintain the formation. Table 3.19 below contains the average $\Delta\mathbf{V}$s per

day for each formation size and orientation. For the cases shown here, the x-axis orientation requires nearly half the $\Delta\mathbf{V}$ magnitudes but only lasts approximately half as long in the error torus.

Table 3.16. $\Delta\mathbf{V}$ Magnitude (m/s) for Formation Size and Formation Pointing on the Inertial X-Axis

Formation Size	$\Delta\mathbf{V}_1$ (m/s)	$\Delta\mathbf{V}_2$ (m/s)	$\Delta\mathbf{V}_3$ (m/s)	$\Delta\mathbf{V}_4$ (m/s)
10 m	3.919×10^{-7}	3.742×10^{-7}	3.792×10^{-7}	3.569×10^{-7}
100 m	1.159×10^{-6}	1.213×10^{-6}	1.384×10^{-6}	1.128×10^{-6}
1 km	3.998×10^{-6}	3.410×10^{-6}	$3.387x\ 10^{-6}$	3.461×10^{-6}

Table 3.17. $\Delta\mathbf{V}$ Magnitude (m/s) for Formation Size and Formation Pointing on the Inertial Y-Axis

Formation Size	$\Delta\mathbf{V}_1$ (m/s)	$\Delta\mathbf{V}_2$ (m/s)	$\Delta\mathbf{V}_3$ (m/s)	$\Delta\mathbf{V}_4$ (m/s)
10 m	7.505×10^{-7}	7.249×10^{-7}	7.270×10^{-7}	$7.341x\ 10^{-7}$
100 m	2.709×10^{-6}	2.731×10^{-6}	2.798×10^{-6}	2.754×10^{-6}
1 km	8.103×10^{-6}	7.982×10^{-6}	$7.716x\ 10^{-6}$	7.785×10^{-6}

Table 3.18. ΔV Magnitude (m/s) for Formation Size and Formation Pointing on the Inertial Z-Axis

Formation Size	$\Delta\mathbf{V}_1$ (m/s)	$\Delta\mathbf{V}_2$ (m/s)	$\Delta\mathbf{V}_3$ (m/s)	$\Delta\mathbf{V}_4$ (m/s)
10 m	7.079×10^{-7}	6.241×10^{-7}	6.322×10^{-7}	6.210×10^{-7}
100 m	2.747×10^{-6}	2.461×10^{-6}	2.421×10^{-6}	2.399×10^{-6}
1 km	8.744×10^{-6}	7.832×10^{-6}	$7.770x\ 10^{-6}$	7.727×10^{-6}

Table 3.19 contains the $\Delta\mathbf{V}$ magnitudes for each formation size and orientation. Similar to the previous case, a general trend emerges that as the size of the orientation increases by an order of magnitude, the $\Delta\mathbf{V}$ requirement to maintain that formation also increases by an order of magnitude. Also, each of the orientations is roughly equivalent in their $\Delta\mathbf{V}$ requirement over a day but the number of $\Delta\mathbf{V}$s performed in a given day is not constant. The orientation pointing in the x-direction requires nearly double the number of

maneuvers than the y-orientation and the z-orientation as can be seen by comparing the time spent in the error corridor contained in Tables 3.13-3.15.

Table 3.19. $\Delta\mathbf{V}$ Magnitude (m/s) per Day for Each Formation and Orientation

Formation Size	X-Pointing	Y-Pointing	Z-Pointing
10 m	1.812×10^{-7}	1.860×10^{-7}	1.726×10^{-7}
100 m	1.890×10^{-6}	1.877×10^{-6}	1.848×10^{-6}
1 km	1.624×10^{-5}	1.724×10^{-5}	1.853×10^{-5}

Figures 3.20-3.28 show the final (of five) segment propagation for the three different formation sizes (10 m, 100 m, 1 km) and the three different orientations (x, y, z-axis). Just like the previous example, each formation had the same relative starting location for the follower spacecraft with the distance magnitude changed (ten meters and one kilometer). The red lines represent the maximum error bound (one centimeter) on either side of the nominal trajectory. The green line represents the reference orbit trajectory. The blue line defines the actual trajectory the follower spacecraft follows over the particular segment. Once again, the $\Delta\mathbf{V}$ magnitudes are well within ESA's microthruster's capabilities.

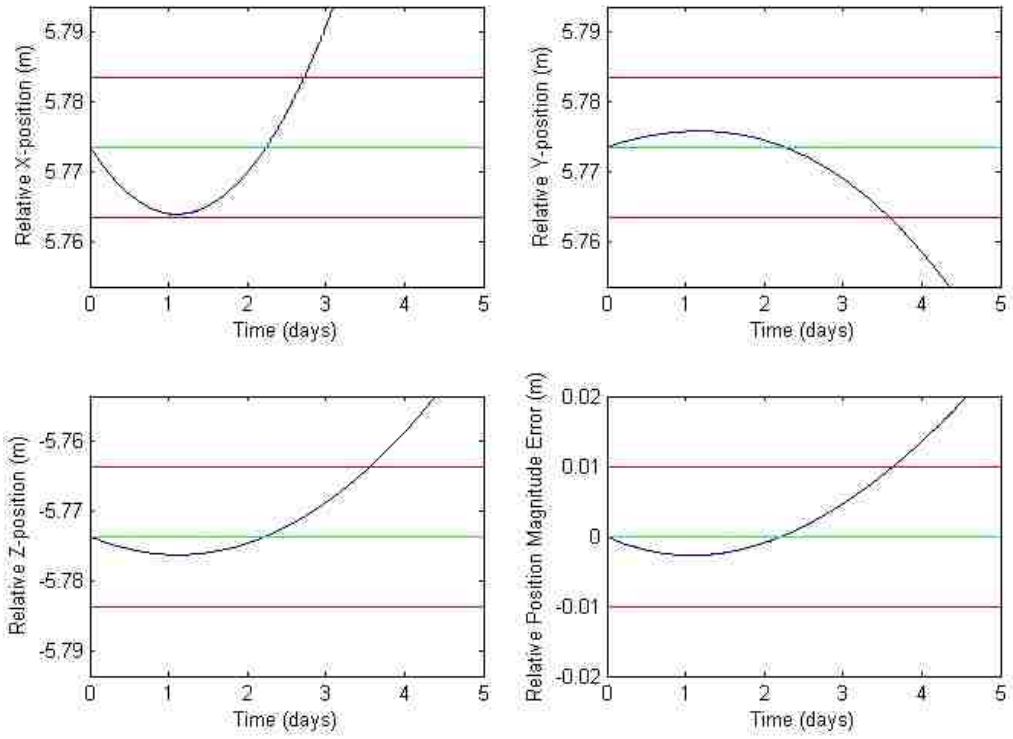

Figure 3.20. 10 m Formation with Formation Pointing along the Inertial X-Axis

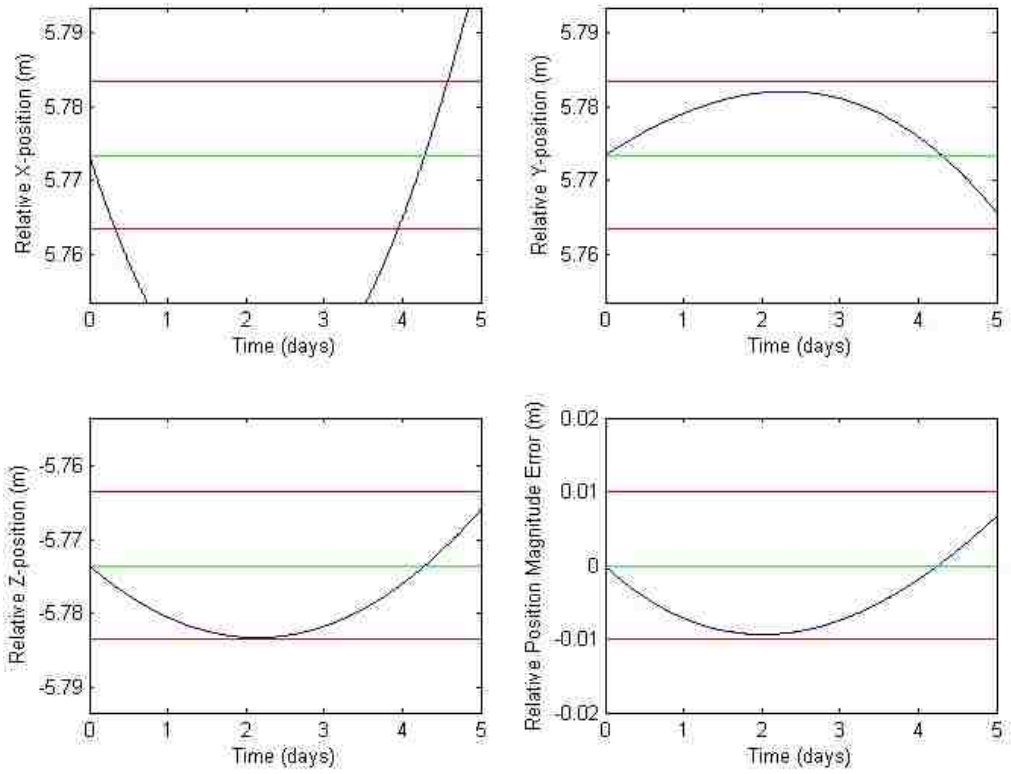

Figure 3.21. 10 m Formation with Formation Pointing along the Inertial Y-Axis

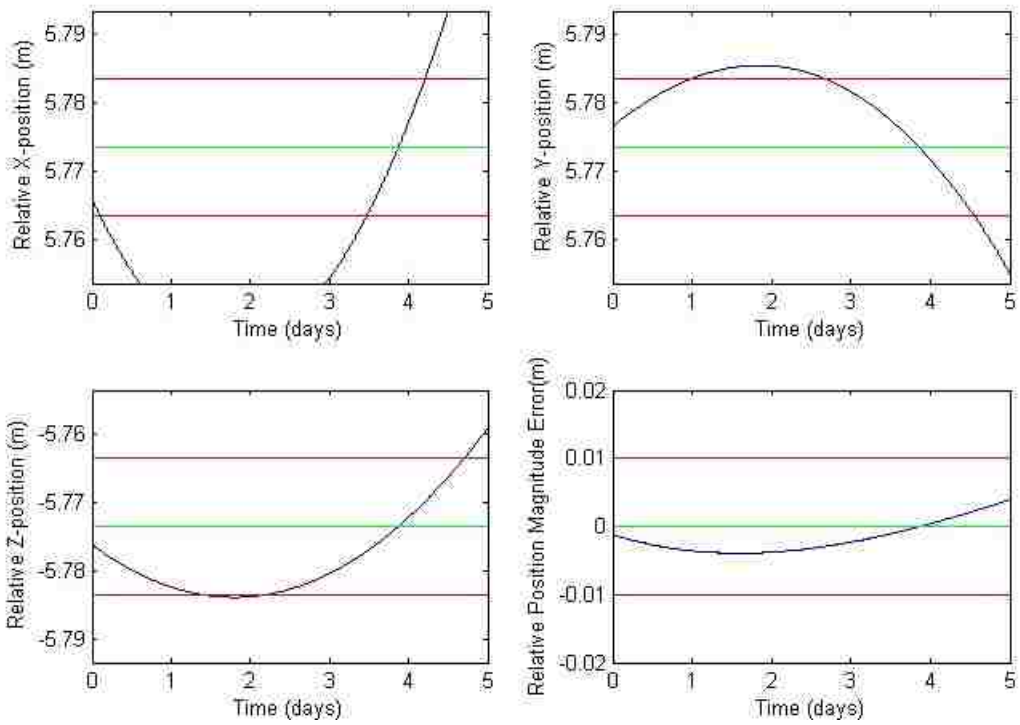

Figure 3.22. 10 m Formation with Formation Pointing along the Inertial Z-Axis

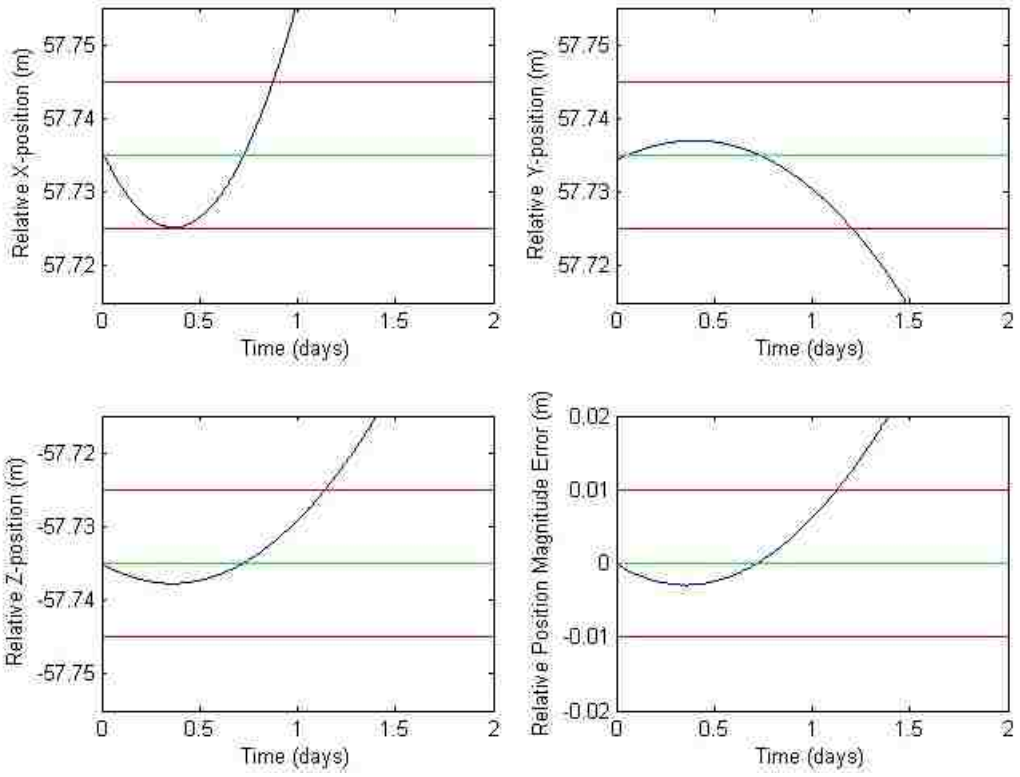

Figure 3.23. 100 m Formation with Formation Pointing along the Inertial X-Axis

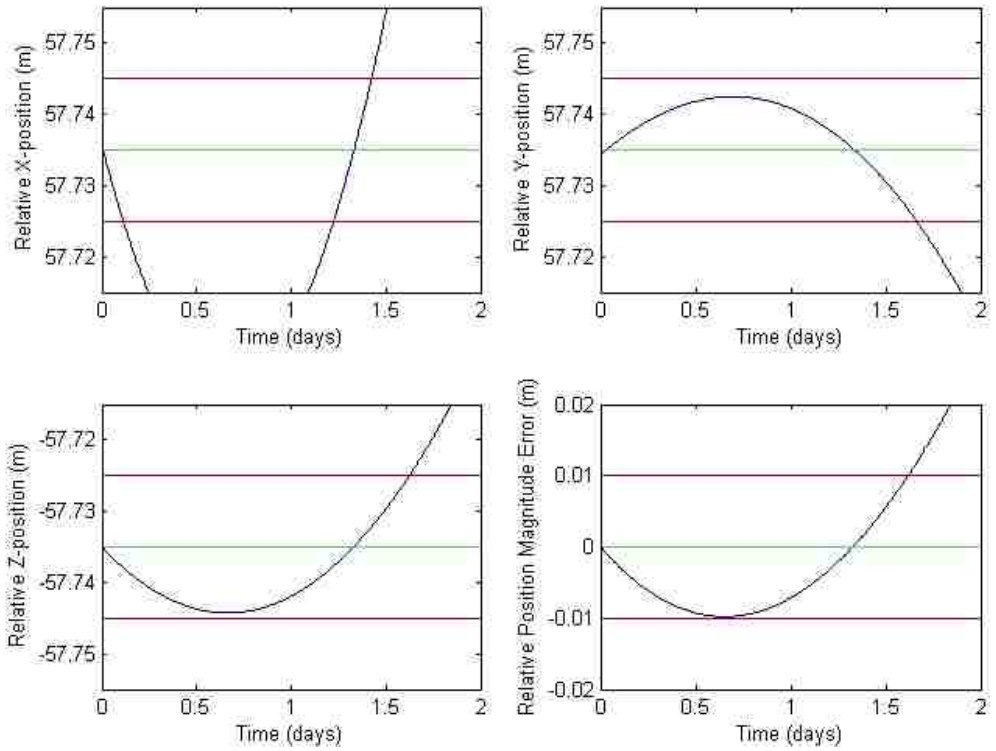

Figure 3.24. 100 m Formation with Formation Pointing along the Inertial Y-Axis

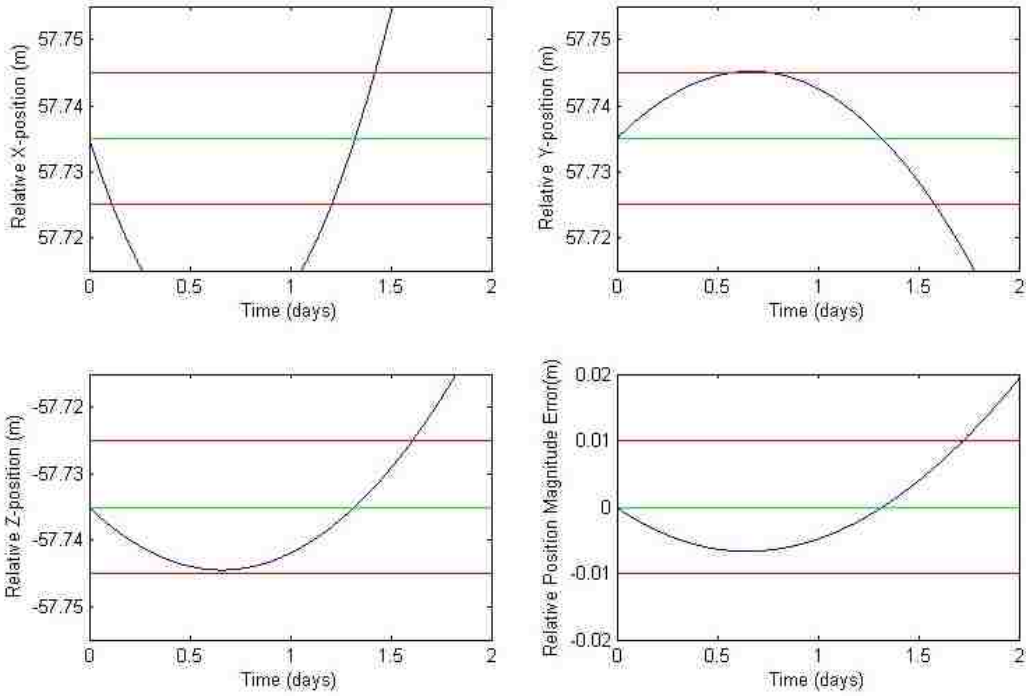

Figure 3.25. 100 m Formation with Formation Pointing along the Inertial Z-Axis

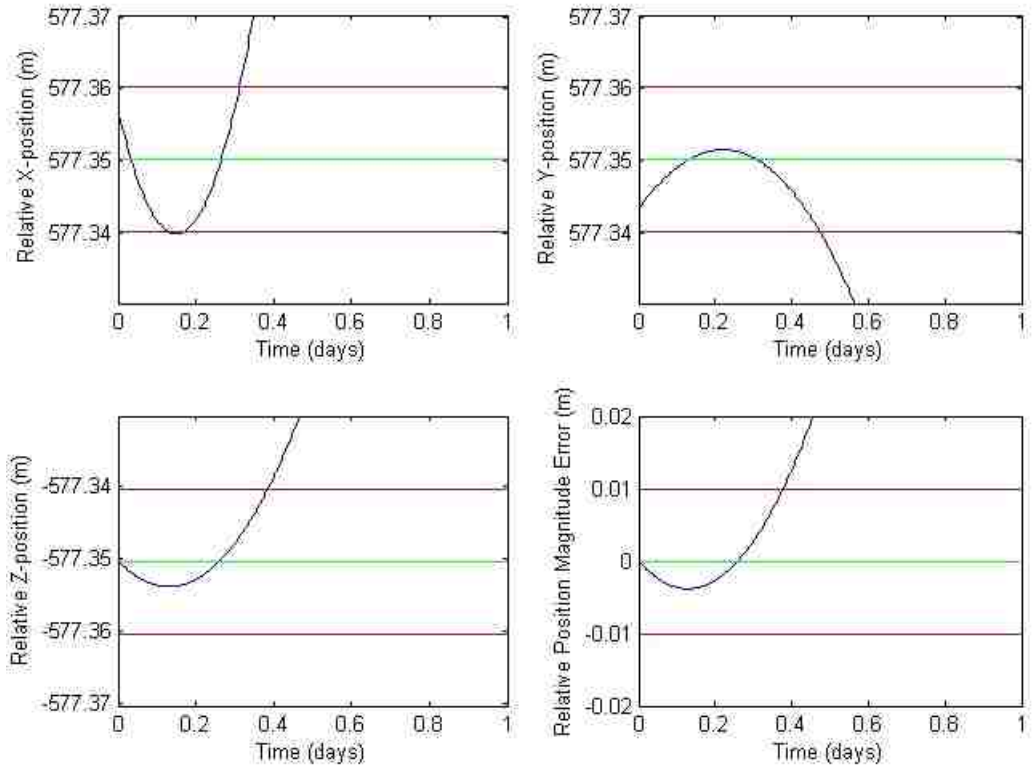

Figure 3.26. 1 km Formation with Formation Pointing along the Inertial X-Axis

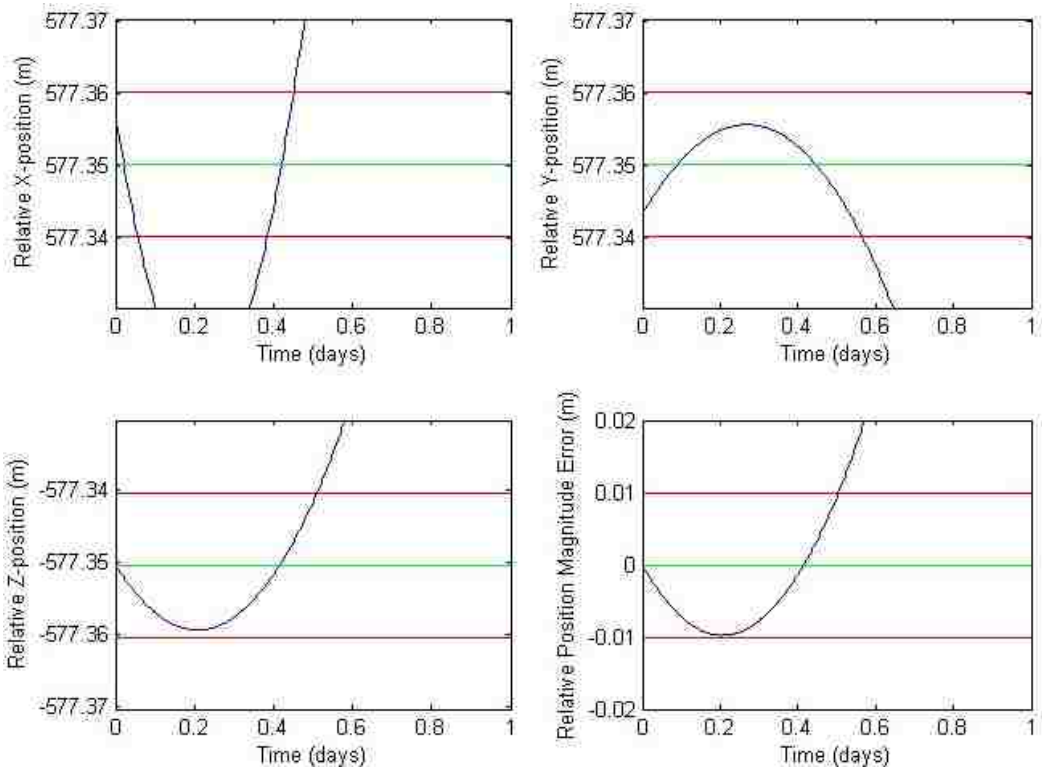

Figure 3.27. 1 km Formation with Formation Pointing along the Inertial Y-Axis

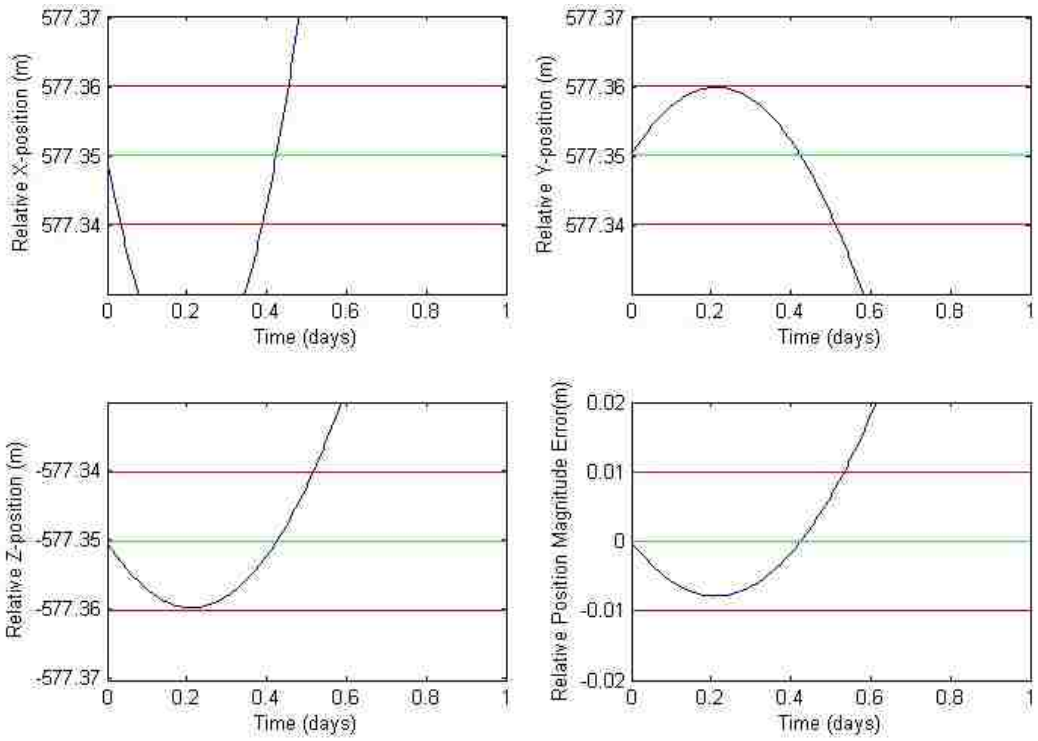

Figure 3.28. 1 km Formation with Formation Pointing along the Inertial Z-Axis

4. CONCLUSIONS

4.1 GENERAL CONCLUSIONS

The original goal of the research was accomplished. A method for finding and exploiting the natural dynamics near a libration point for formation flight was determined. Various formations types were examined to determine the feasibility of natural dynamics on the formations.

Three different formation types were examined. For all cases, it was assumed the leader spacecraft was on a known halo orbit about the L_2 libration point for the Sun-Earth/Moon three-body system. The first formation examined had a follower spacecraft placed in a halo orbit relative to the leader spacecraft. While natural follower halo orbits could be found, multiple followers could not be placed on the same relative halo orbit trajectory at varying initial positions. Relative halo orbits do not lend themselves to formations with large numbers of spacecraft if the natural dynamics are to be exploited. Instead, continuous control would be required to maintain any given formation with follower spacecraft in relative halo orbits.

The second formation type examined was the case with a follower spacecraft in a fixed position relative to the leader spacecraft. It was required that the follower spacecraft remain in the exact same position relative to the follower spacecraft with respect to the rotating frame at all times. Due to the fact that the leader spacecraft's position was considered a known quantity at all times, it was assumed that the nominal orbit of the follower spacecraft in its fixed position was also a known. An error tolerance of one centimeter from the nominal orbit was used for all cases consistent with the NASA Goddard Spaceflight Center research announcement[44]. Other error tolerances could be implemented for any formation size or geometry.

A simple discrete $\Delta\mathbf{V}$ control method was used to compare the various $\Delta\mathbf{V}$ magnitudes and overall fuel consumption for a given formation geometry while examining the time spent in the error "sphere." The smallest $\Delta\mathbf{V}$ occurred for the ten-meter formation (with one centimeter error tolerance) and it was on the order of $1\text{x}10^{-7}$ m/s, well within the feasibility of the ESA microthruster.

The third and final formation type examined was the follower spacecraft constrained to a paraboloid with the leader spacecraft at the focus. The follower spacecraft was constrained to stay within an error "torus." The same discrete $\Delta\mathbf{V}$ control method was implemented for this case. Similar to the fixed-position formation, the smallest $\Delta\mathbf{V}$ was on the order of $1x10^{-7}$ m/s, also well within range of the ESA microthruster.

4.2 FUTURE DEVELOPMENTS

Considering the wide scope of the present research, a additional research can be undertaken in multiple areas.

Considerable research has focused on the Sun-Earth/Moon L_2 libration point, but placing the leader spacecraft at a different libration point for a different three-body system and examining the effects of the natural dynamics on various formations at these different libration points and systems would be valuable. Additionally, a parametric study on various leader spacecraft orbits and their influence on natural formation dynamics could be performed. The leader spacecraft could be put on larger or smaller halo orbits or on Lissajous orbits near a libration point.

The size and geometry of formations as well as the number of spacecraft in the formation could be explored in more detail. The present research could be used as a starting point for a mission with a specific formation size, geometry and number of spacecraft.

Further research could be done in examining in more detail the "neighborhoods" that govern the "good" natural dynamics and the ability to exploit these neighborhoods for large formations, rather than just focusing on a leader spacecraft and one follower. Instead of examining the natural dynamics of a single follower spacecraft with respect to a leader, one could examine the influence of the natural dynamics on an entire formation and determine favorable geometries and initial conditions that lend themselves to maintaining a formation over a long period of time (minimizing fuel costs). In addition, a formal analytical solution to determine the "neighborhoods" could also be of use in future research.

A final point of possible future work would be to explore the process of reorienting of the various formations while attempting to utilize the natural dynamics as much as possible. The NASA Goddard Spaceflight Center research announcement stated a goal of a formation slewing as much as twenty degrees per day to acquire a new science target. Methods could be developed to exploit the natural dynamics near a libration point to accomplish this task.

APPENDIX A:
LEADER SPACECRAFT

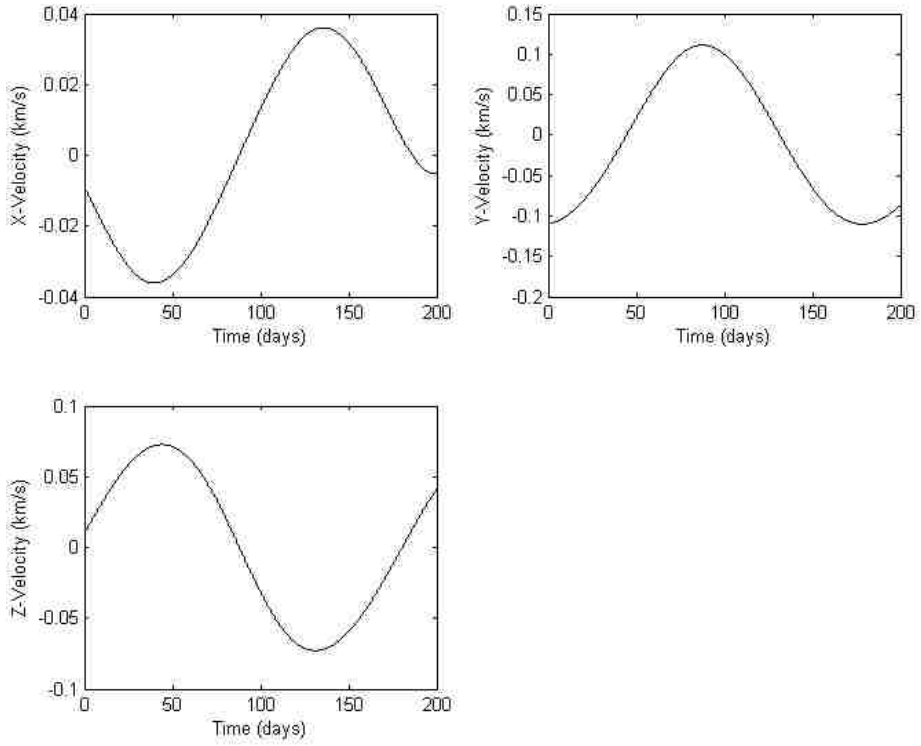

Figure A.1. Leader Spacecraft Velocity Profiles (km/s) vs Time (days)

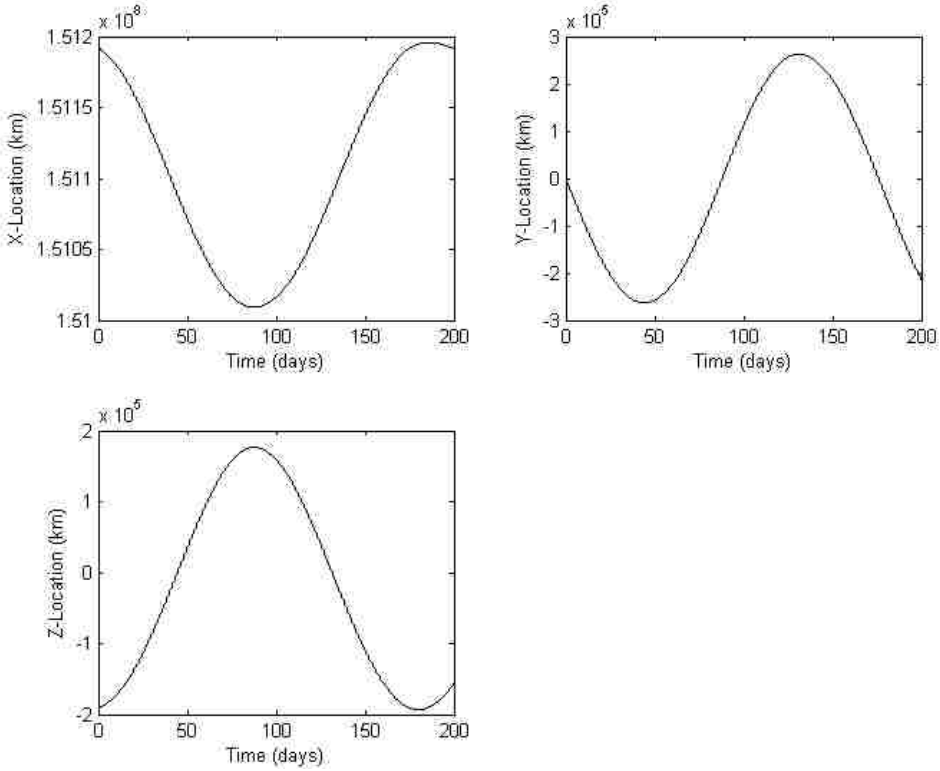

Figure A.2. Leader Spacecraft Position (km) vs Time (days)

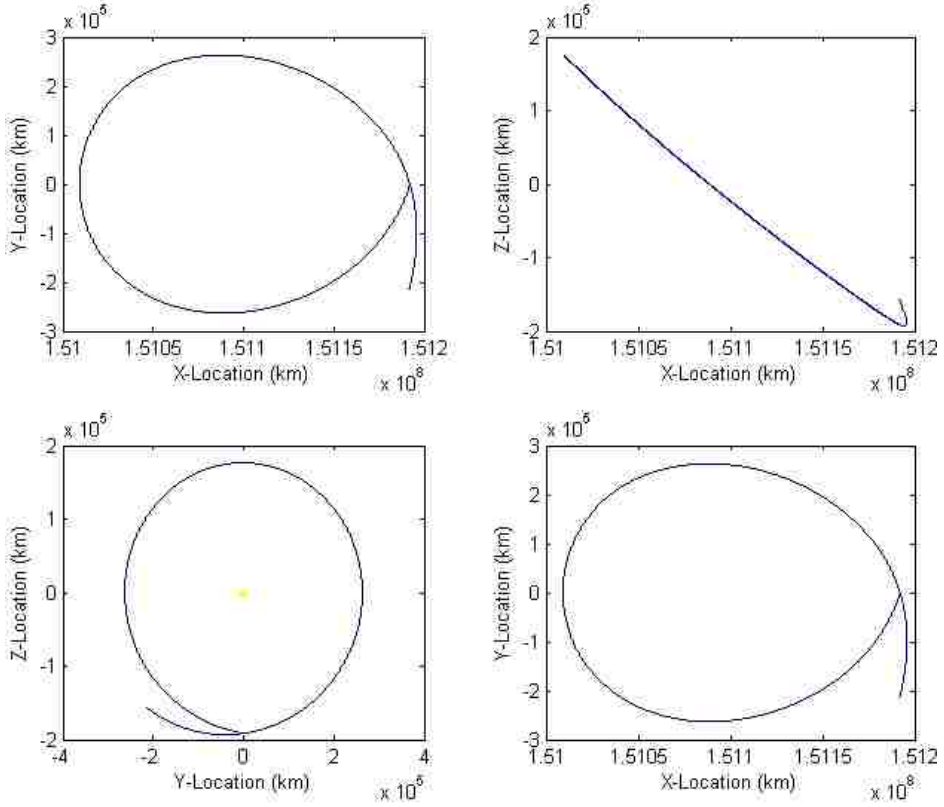

Figure A.3. Two-Dimensional Halo Orbit Projections for the Leader Spacecraft

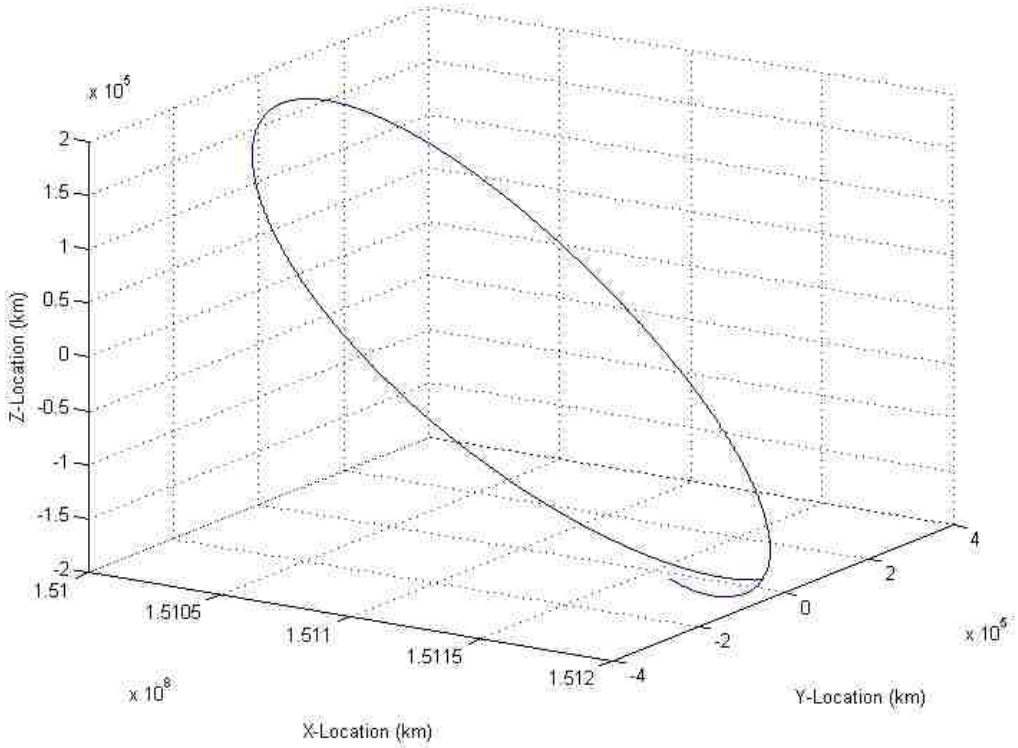

Figure A.4. Three-Dimensional View of Leader Spacecraft Halo Orbit

APPENDIX B:
FOLLOWER SPACRAFT INITIAL POSITIONS

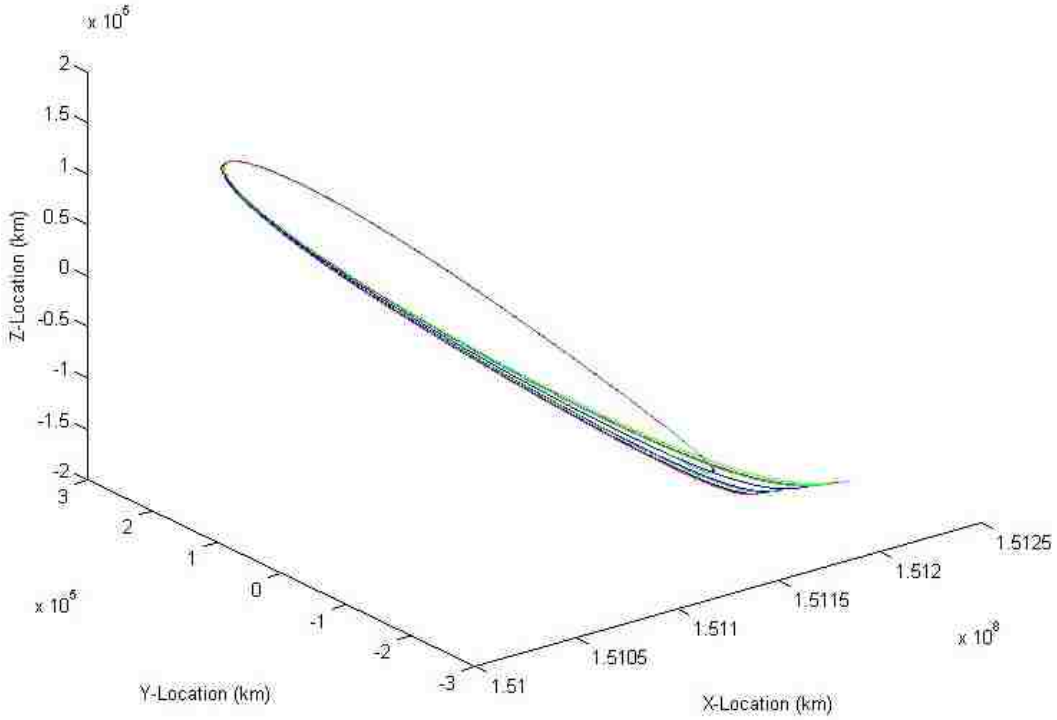

Figure B.1. Three-Dimensional Halo Orbits of Various Follower Initial Positions

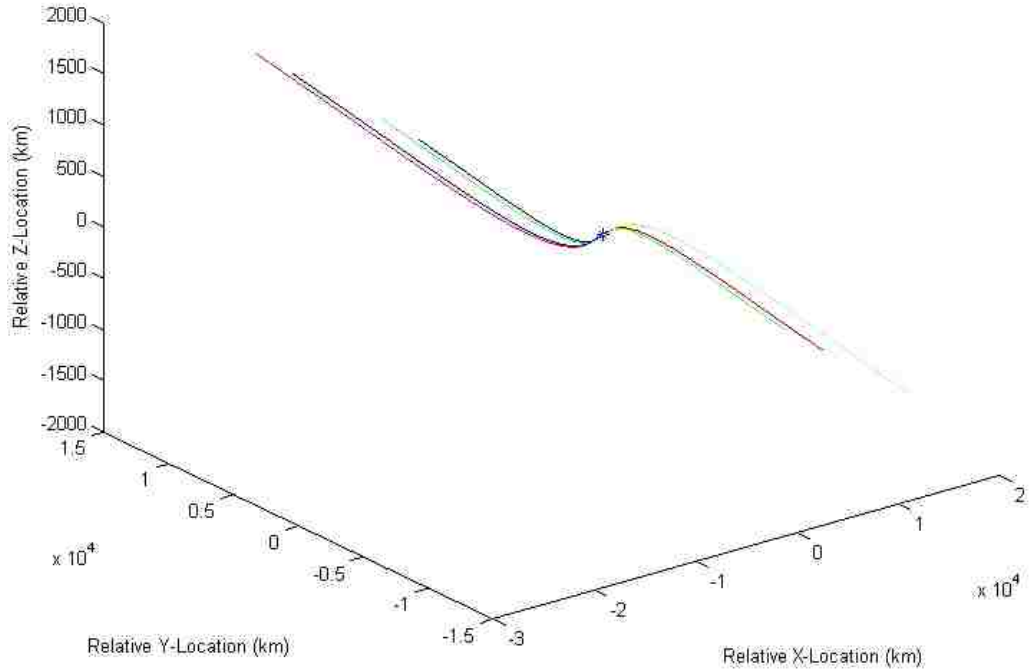

Figure B.2. Three-Dimensional Relative Orbits of Various Follower Initial Positions

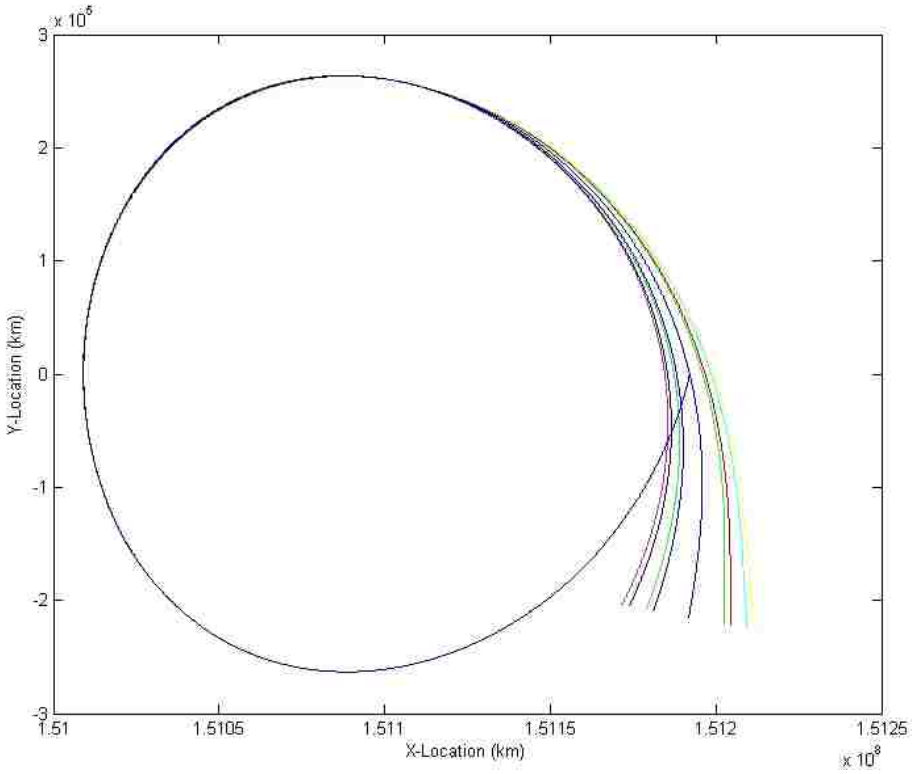

Figure B.3. Two-Dimensional Projection of Various Follower Initial Positions

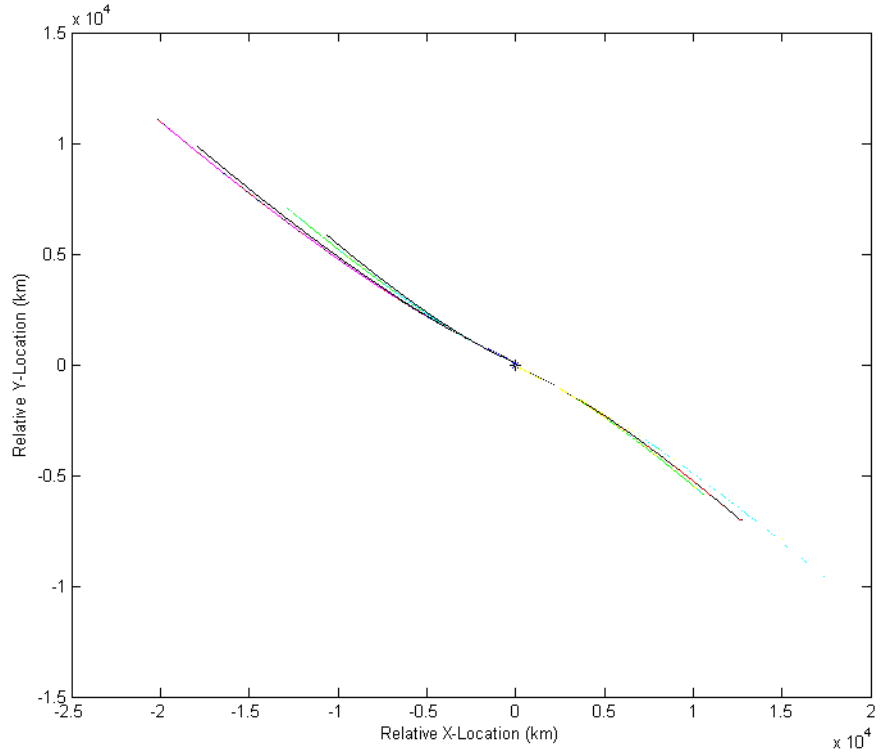

Figure B.4. Two-Dimensional Relative Orbits of Various Follower Initial Positions

BIBLIOGRAPHY

[1] Distributed Space Systems," July 28, 2004, http://gsfctechnology.gsfc.nasa.gov/focusAreas/dss.htm.

[2] Distributed Space Systems," July 28, 2004, http://ses.gsfc.nasa.gov/ses_data_2002/020402_Leitner_Abstract.htm .

[3] John D Monnier, "Optical Interferometry in Astronomy," *Reports on Progress in Physics 66* (2003) 789-857

[4] Szebehely, V., *Theory of Orbits: The Restricted Problem of Three Bodies*, Academic Press, New York, 1967.

[5] Farquahar, R.W., and Kamel, A.A., "Quasi-Periodic Orbits About the Translunar Libration Point," *Celestial Mechanics*, Vol. 7, 1973, pp. 458-473.

[6] David L. Richardson and Noel D. Cary, "A Uniformly Valid Solution for Motion about the Interior Libration Point of the Perturbed Elliptic-Restricted Problem," American Astronautical conference paper AAS 75-021, 1975.

[7] David L. Richardson, "Analytic Construction of Periodic Orbits About the Collinear Points," *Celestial Mechanics,* Vol. 22, 1980, pp. 241-253.

[8] David L. Richardson, "A Note on a Lagrangian Formulation for Motion About the Collinear Points," *Celestial Mechanics,* Vol. 22*,* 1980, pp. 231-236.

[9] David L. Richardson, "Halo Orbit Formulation for the ISEE-3 Mission," AIAA paper 1979-80-4122, 1979.

[10] K. C. Howell, "Families of Orbits in the Vicinity of the Collinear Libration Points," paper AAS 98-4465, 1998.

[11] K. C. Howell and H. J. Pernicka, "Numerical Determination of Lissajous Trajectories in the Restricted Three-Body Problem," AIAA paper 1986-2002, 1986.

[12] David Cielaszyk and Bong Wie, "New Approach to Halo Orbit Determination and Control," *Journal of Guidance, Control and Dynamics*, Vol. 19, No. 2, 1996, pp 266-273.

[13] Pini Gurfil and Dani Meltzer, "Stationkeeping on Libration Point Orbits in the Elliptic Restricted Three-Body Problem," AIAA paper 2006-6035, 2006.

[14] A. Rahmani, M.A. Jalali, and S.H. Pourtakdoust, "Optimal Approach to Halo Orbit Control," AIAA paper 2003-5748, 2003.

[15] D.W. Dunham and C.E. Roberts, "Stationkeeping Techniques for Libration-Point Spacecraft," *The Journal of the Astronautical Sciences,* Vol. 49, No. 1**,** pp. 127-144, 2001.

[16] de Querirox, M.S., Kapila, V., and Yan, Q., "Adaptive Nonlinear Control of Multiple Spacecraft Formation Flying," *Journal of Guidance, Control, and Dynamics*, Vol. 23, No. 3, 2000, pp. 385-390.

[17] Inalhan G., Tillerson, M., and How, J.P., "Relative Dynamics and Control of Spacecraft Formations in Eccentric Orbits," *Journal of Guidance, Control, and Dynamics*, Vol. 25, No. 1, 2003, pp. 48-59.

[18] Sparks, A., "Linear Control of Spacecraft Formation Flying," AIAA Paper 2000-4438, AIAA Guidance, Navigation, and Control Conference, Denver, CO, August 14-17, 2000.

[19] Campbell, M.E., "Planning Algorithm for Multiple Spacecraft Clusters," *Journal of Guidance, Control, and Dynamics*, Vol. 26, No. 5, 2003, pp. 770-780.

[20] "Glossary of Goddard Technology Management Office (GTMO) Terms," June, 10, 2004, http://gsfctechnology.gsfc.nasa.gov/focusAreas/glossary.htm.

[21] "Distributed Space Systems," July 28, 2004, http://gsfctechnology.gsfc.nasa.gov/focusAreas/dss.htm.

[22] Carpenter, J.R., Leitner, J.A., Folta, D.C., and Burns, R.D., "Benchmark Problems for Spacecraft Formation Flying Missions," AIAA Paper 2003-5364, AIAA Guidance, Navigation, and Control Conference and Exhibit, Austin, TX, August 11-14, 2003.

[23] Bristow, J., Folta, D., and Hartman, K., "A Formation Flying Technology Vision," AIAA Paper 2000-5194, AIAA Space 2000 Conference and Exposition, Long Beach, CA, September 19-21, 2000.

[24] Vadali, S.R., Bae, H.-W., and Alfriend, K.T., "Design and Control of Libration Point Spacecraft Formations," AAS Paper 04-161, 14th AAS/AIAA Space Flight Mechanics Conference, Maui, HI, February 8-12, 2004 .

[25] Scheeres, D.J., Hsiao, F.-Y., and Vinh, N.X., "Stabilizing Motion Relative to an Unstable Orbit: Applications to Spacecraft Formation Flight," *Journal of Guidance, Control, and Dynamics*, Vol. 26, No. 1, 2003, pp. 62-73.

[26] Wiesel, W.E., "Optimal Impulsive Control of Relative Spacecraft Motion," *Journal of Guidance, Control, and Dynamics*, Vol. 26, No. 1, 2003, pp. 74-78.

[27] Barden, B.T., Howell, K.C., and Lo, M.W., "Application of Dynamical Systems Theory to Trajectory Design for a Libration Point Mission," AIAA/AAS Astrodynamics Conference, San Diego, CA, July 29-31, 1996, Collection of Technical Papers (A96-34712 09-12).

[28] Mitchell, J.W. and Richardson D.L., "Invariant Manifold Tracking for First-Order Nonlinear Hill's Equations," *Journal of Guidance, Control, and Dynamics*, Vol. 26, No. 4, 2003, pp. 622-627.

[29] Marchand, B.G., Howell, K.C., "Formation Flight Near L_1 and L_2 in the Sun-Earth/Moon Ephemeris System Including Solar Radiation Pressure," AAS Paper 03-596, AAS/AIAA Astrodynamics Specialist Conference, Big Sky Resort, Big Sky, MT, August 3-7, 2004.

[30] Marchand, B.G. and Howell, K.C., "Aspherical Formations Near the Libration Points in the Sun-Earth/Moon Ephemeris System," AAS Paper 04-157, 14th AAS/AIAA Space Flight Mechanics Conference, Maui, HI, February 8-12, 2004.

[31] Pernicka, H.J., Carlson, B.A., and Balakrishnan, S.N. "Spacecraft Formation Flight About Libration Points Using Impulsive Maneuvering," *Journal of Guidance, Control, and Dynamics*, Vol. 29, No. 5, September-October 2006, pp. 1122-1130.

[32] Ziemer, J., Gamera-Costano, et al, "Colloid Micro-Newton Thruster Development for ST7-DRS and LISA Missions," AIAA Paper 2005-4265, 41st AIAA/ASME/SAE/ASEE Joint Propulsion Conference and Exhibit, Tucson, AZ, July 10-13, 2005.

[33] "Small Engine For the Big Job of Testing Theory of Relativity," April 10th, 2009, http://www.universetoday.com/2009/04/10/small-engine-for-the-big-job-of-testing-theory-of-relativity/

[34] Xin, M., Balakrishnan, S.N., Pernicka, H.J., "Position and Attitude Control of Deep-Space Spacecraft Formation Flying via Virtual Structure and Theta-D Technique," *Journal of Dynamic Systems, Measurement, and Control,* accepted and to appear.

[35] Xin, M., Balakrishnan, S.N., Pernicka, H.J., "Multiple Spacecraft Formation Control with θ-D Method," *IET Control Theory and Applications,* March 2007, Volume 1, Issue 2, pp. 485-493.

[36] Samantha I. Infield, Scott B. Josselyn, Walter Murray, and I. Michael Ross, "Design and Control of Libration Point Spacecraft Formations," *Journal of Guidance, Control, and Dynamics*, Vol. 30, No. 4, 2007, pp. 899-909.

[37] Guillaume Collange, Jesse Leitner, “Spacecraft Formation Design Near the Sun-Earth L_2 Point,” AIAA paper 2004-4781.

[38] Kathryn A. Caitlin, Craig A. McLaughlin, "Relative Motion of Two Spacecraft Near the Earth-Moon Triangular Libration Points," AIAA paper 2004-4743.

[39] Kathryn A. Catlin, Craig A. McLaughlin, "Earth-Moon Triangular Libration Point Spacecraft Formations," *Journal of Spacecraft and Rockets* Vol. 44, No. 3, May-Jun 2007.

[40] Segerman, A.M., Zedd, M.F., “Preliminary Planar Formation-Flight Dynamics Near Sun-Earth L2 Point,” AAS/AIAA Space Flight Mechanics Meeting, Ponce, Puerto Rico, Paper 03-133, February 9-13, 2003.

[41] Luquette, R. J., Leitner, J. A., Gendreau, K., and Sanner, R. M., “Formation Control for the MAXIM and MAXIM Pathfinder Missions,” NASA Goddard Space Flight Center, Greenbelt, MD, 2002.

[42] Lagadec, K., Lebas, J., and Ankersen, F., “Precision Formation Flying for the the Darwin Interferometer,” 5th International ESA Conference on Spacecraft Guidance, Navigation and Control System, 2002.

[43] Marchand, B.G., Howell, K.C., “Formation Flight Near L_1 and L_2 in the Sun-Earth/Moon Ephemeris System Including Solar Radiation Pressure,” AAS Paper 03-596, AAS/AIAA Astrodynamics Specialist Conference, Big Sky Resort, Big Sky, MT, August 3-7, 2004.

[44] Leitner, J., “Formation Navigation, Control, and Mission Design Algorithms,” NASA Goddard Spaceflight Center NRA-03-GSFC/AETD-01, February 7, 2003

VITA

Douglas (Doug) Robert Tolbert was born on July 16, 1982 to Steve and Rosalie Tolbert. He graduated from Hardin County High School in May of 2000 and enrolled at the University of Missouri-Rolla that fall. In May of 2004, he graduated with a Bachelors of Science degree in Aerospace Engineering. Doug got married on June 4, 2005 to Stephanie Hiehle of North Carolina. He received a Masters of Science degree in Aerospace Engineering in December of 2005. He successfully earned his Ph.D. in aerospace engineering at UMR (now called Missouri University of Science and Technology) in August of 2009. While at UMR, Doug was a member of many organizations including the Advanced Aero Vehicle Group, the UMR Ultimate Frisbee Team, Missouri-Rolla Spacecraft Design Team, AIAA, and Sigma Gamma Tau. Doug was also a co-op student at the NASA Langley Research Center the summer and fall of 2002, the summer of 2003, and the summer of 2004.